Prolate and oblate band structures in odd-odd ^{186,188}Au

V. P. Janzen,* Z.-M. Liu,† M. P. Carpenter,‡ L. H. Courtney,§ H.-Q. Jin, A. J. Larabee,** and L. L. Riedinger
Department of Physics and Astronomy, University of Tennessee, Knoxville, Tennessee, 37996

J. K. Johansson, D. G. Popescu,†† and J. C. Waddington
Tandem Accelerator Laboratory, McMaster University, Hamilton, Canada L8S 4K1

S. Monaro and S. Pilotte‡‡
Laboratoire de Physique Nucléaire, Université de Montréal, Montréal, Canada H3C 3J7

F. Dönau§§
Joint Institute for Heavy Ion Research, Oak Ridge, Tennessee, 37831
(Received 8 March 1991)

High-spin states have been populated in odd-odd ^{186,188}Au via the heavy-ion ^{171,173}Yb(^{19}F,4n) reactions at 93–94 MeV. Rotational bands built on 11^- oblate $\nu i_{13/2}^{-1} \otimes \pi h_{11/2}^{-1}$ structures have been observed in both nuclei, similar to those reported in $^{190-194}$Au. Two new strongly coupled bands in ^{186}Au are interpreted as prolate $\pi h_{9/2} \otimes \nu i_{13/2}$ and $\pi i_{13/2} \otimes \nu i_{13/2}$ configurations. Based on blocking arguments a band crossing in the latter structure is attributed to the alignment of $h_{9/2}$ protons. Measured $B(M1; I \rightarrow I-1)/B(E2; I \rightarrow I-2)$ ratios are compared to predictions of the Dönau and Frauendorf geometrical formalism extended to odd-odd cases.

PACS number(s): 21.10.Re,27.70.+q,25.70.−z

I. INTRODUCTION

At low to intermediate values of angular momentum the two dominant nuclear structure features of the $A \simeq 180$ region are (i) the dynamic competition between prolate and oblate shapes, and (ii) the deformation-driving effects and band crossing characteristics of influential high-j quasiparticle orbitals under rotation. Both of these features have been extensively studied for odd- and even-A cases in the light Pt-Au-Hg region [1–10] These include experimental investigations of high-spin states in ^{185}Au [1], ^{183}Ir [4,5], ^{187}Au [6], ^{184}Pt [7], ^{183}Pt [8], ^{185}Pt [4,9], and ^{187}Hg [10]. Nevertheless, a knowledge of the odd-odd Au nuclei is critical if we wish to answer the remaining questions concerning, for example, the competition between $\nu i_{13/2}$ and $\pi h_{9/2}$ rotational band crossings. This can be most clearly illustrated if it were possible to isolate a band comprised of *both* quasiparticles thought to be responsible for the band crossings observed in neighboring nuclei. The prolate $\pi h_{9/2} \otimes \nu i_{13/2}$ configuration, reported here in ^{186}Au and recently in ^{184}Ir [11], provides a striking example of this. It is significant that this is the only configuration observed in the $N = 105 - 107$ isotones not displaying any alignment gain below a rotational frequency $\hbar\omega = 0.3$ MeV. Discussion of this double blocking in other odd-odd nuclei in the region is given by Kreiner *et al.* [12,13].

In addition, an analysis of the γ-ray branching ratios can provide a very useful test of our understanding of transition matrix elements, which are sensitive to the nuclear shape, quasiparticle composition, and rotational characteristics such as signature splitting. The present work outlines an extension of the semiclassical formalism of Dönau and Frauendorf [14,15] to odd-odd cases.

There is already a significant amount of low- to medium-spin data regarding odd-odd prolate structures in the Ir and Re isotopic chains (e.g., Kreiner *et al.* [11,16]). However, less is known about excited states of the doubly odd Au nuclides. Oblate band structures in the $A = 190, 192, 194$ isotopes of Au have been studied via in-beam spectroscopy by Neskakis *et al.* [17,18]. From resonance-ionization mass-spectrometry work ^{186}Au is known [3] to be the heaviest $Z = 79$ isotope which is prolate in its ground state, with the $A \geq 187$ nuclides

*Present address: AECL Research, Chalk River Laboratories, Chalk River, Ontario, Canada K0J 1J0.
†Present address: Lanzhou University, Lanzhou, P.R. China.
‡Present address: Argonne National Laboratory, Physics Division, 9700 Cass Avenue, Argonne, IL 60439.
§Present address: The Science Alliance, University of Tennessee, Knoxville, TN 37996
**Present address: Physics Department, Buena Vista College, Storm Lake, Iowa, USA 50588.
††Present address: Institut de Physique Nucléaire, 91406 Orsay, France.
‡‡Present address: Department of Physics, University of Ottawa, Ottawa, Ontario, Canada, K1N 6N5.
§§On leave from the Zentralinstitut für Kernforschung Rossendorf, DDR-8051 Dresden, Federal Republic of Germany.

exhibiting small oblate deformations. Rotational bands in the transitional ^{186,188}Au nuclei can therefore be expected to reflect the competition between two distinct nuclear shapes.

II. EXPERIMENTAL PROCEDURE

The present work is the result of a series of experiments performed at the McMaster Tandem Accelerator Laboratory, which included γ-γ coincidence, γ-ray angular distribution, and γ-γ-t measurements. Limited excitation functions, using ^{19}F beams of 92 to 97 MeV supplied by the FN tandem accelerator, were also measured in order to determine optimum bombarding energies. The ^{171,173}Yb(^{19}F,4n)^{186,188}Au reactions were used at beam energies of 93 to 94 MeV for all of the following measurements. Enriched 2-mg/cm^2 Yb targets were backed with approximately 8 mg/cm^2 of ^{208}Pb, which served to stop the recoiling Au nuclei. Beam particles were stopped in a 100-mg/cm^2 Pb foil behind the target.

A. γ-γ coincidence measurements

For the standard coincidence experiments two arrays of γ-ray detectors were used. The first consisted of five coaxial Ge detectors ranging in efficiency from 11% to 26% (relative to a 7.6×7.6-cm NaI crystal at 1.33-MeV) and in peak resolution from 1.9 to 2.5 keV FWHM for the ^{60}Co 1.33-MeV γ ray. The detectors, which had no suppression for Compton-scattered γ rays, were positioned at angles of approximately ±105°, ±40°, and 0° with respect to the beam axis at distances of 8 to 10 cm from the target. Thin Cd-Cu absorbers were placed in front of the crystals to reduce the count rate due to x rays. Thick Pb shields were used over the other outer surfaces to reduce the probability of Ge-to-Ge γ-ray scattering. Standard electronic techniques were used to measure two- or higher-fold coincidences, with an overall resolving time of approximately 100 ns. The detector gains were monitored on-line for later correction.

Five large (12.7×15.2 cm) NaI detectors plus one 7.6×7.6 cm BGO detector made up a second array, which served as a multiplicity filter. The filter elements were placed between the Ge positions at distances similar to those of the Ge units, and were well shielded from each other by thick Pb and Cd absorbers, as well as on their front surfaces by thin layers of Pb and Cd to minimize the number of x rays detected.

An acceptable event consisted of a Ge-Ge twofold coincidence plus a multiplicity filter coincidence, or alter-

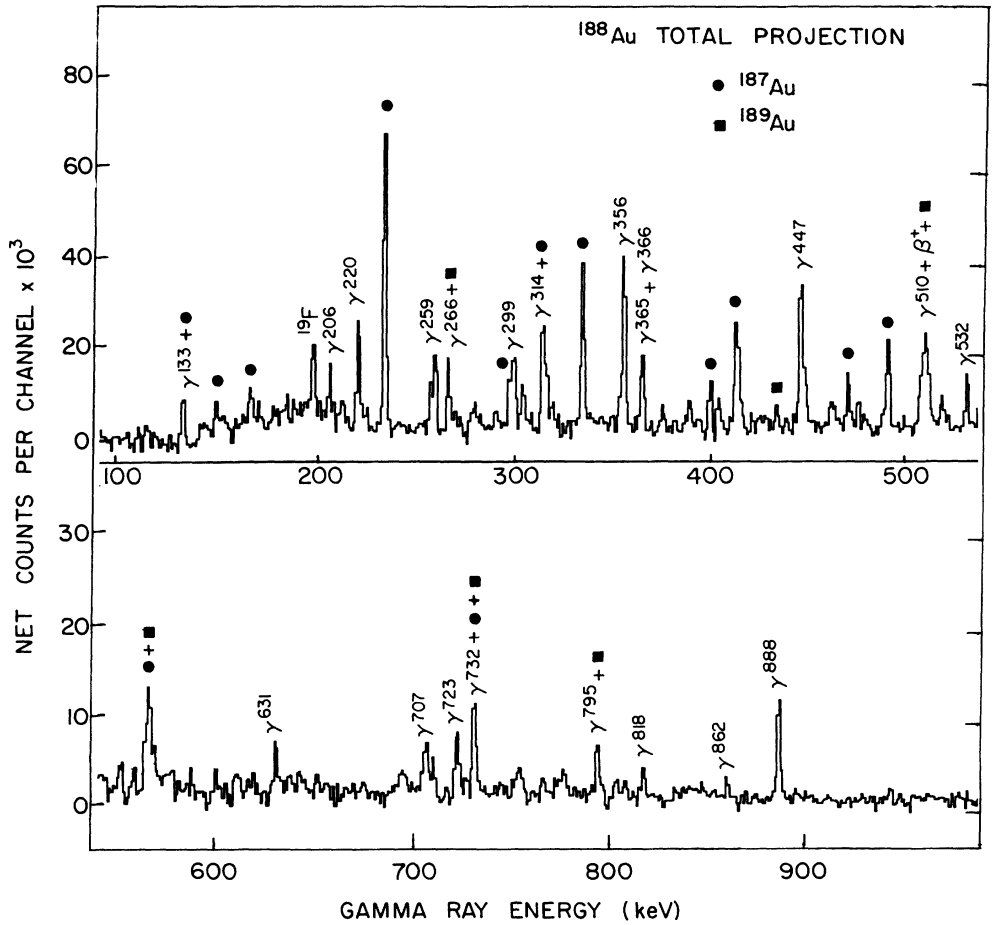

FIG. 1. Total γ-ray coincidence spectrum following background subtraction for the ^{173}Yb + ^{19}F reaction at 93 MeV, gated by at least a twofold coincidence in the NaI multiplicity filter. Prominent peaks corresponding to transitions in ^{188}Au are marked by their energies in keV.

natively a threefold Ge-Ge coincidence. Approximately 65×10^6 (^{186}Au) and 100×10^6 (^{188}Au) coincidences were acquired in the two experiments. γ-ray energy information was written event by event onto magnetic tape and sorted later into 1024-by-1024-channel matrices, at which time the data were adjusted for individual detector gain differences. Background was subtracted from the entire matrix using the method of Palameta and Waddington [19]. Coincidence spectra were then extracted for many of the peaks in the total projections. Figures 1 and 2 show the total projections for the ^{188}Au and ^{186}Au matrices, respectively, while Figs. 3 and 4 contain several gated spectra from each nucleus. Due to the high intensities of γ rays arising from competing $3n$ and $5n$ reaction channels, and the relatively low resolution dictated by the 1024-channel matrix limitation, the projection spectra and some of the gated spectra contain significant numbers of contaminant peaks.

The γ rays identified with ^{188}Au and ^{186}Au are listed in Tables I and II. As a result of interfering peaks, in a large number of cases the angular distribution measurements (see below) were unable to accurately determine γ-ray intensities, and then I_γ values were evaluated using coincidence spectra. Corrections were made for the relative efficiency of the Ge detector array, based upon measured γ-ray intensities from a ^{152}Eu source.

B. γ-ray angular distributions

A separate experiment was performed in order to measure the angular distributions of the more intense transitions. Five coaxial Ge detectors, having similar characteristics to those described in the previous section, were positioned at angles of 90°, 60°, 45°, 30°, and −10° with respect to the beam axis, 10 cm from the target. The multiplicity filter elements were positioned symmetrically about the beam axis, to reduce possible angular correlation effects. γ-ray spectra, gated by a filter coincidence, were acquired for each Ge detector. For the ^{173}Yb(^{19}F,xn) reaction, intensities of the clean strong 233.4-keV $\frac{13}{2}^- \rightarrow \frac{9}{2}^-$ transition in ^{187}Au [6,20] were normalized at each angle to a theoretical $E2$ angular distribution, based on a Gaussian population distribution of the magnetic substates population characterized by $\sigma/J = 0.25$ [21]. Then that set of normalization factors, adjusted at other energies for the measured differences

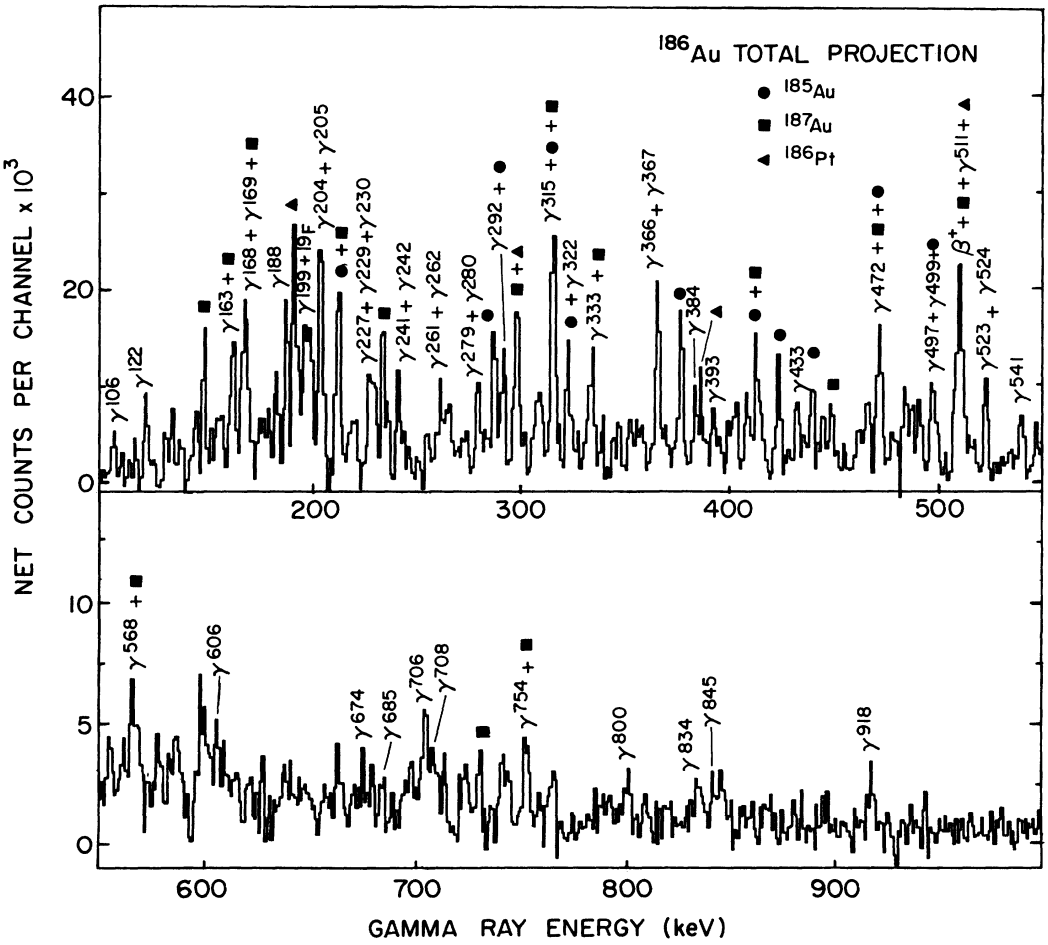

FIG. 2. Total γ-ray coincidence spectrum following background subtraction for the ^{171}Yb + ^{19}F reaction at 94 MeV, gated by at least a twofold coincidence in the NaI multiplicity filter. Prominent peaks corresponding to transitions in ^{186}Au are marked by their energies in keV.

between individual detector efficiencies, was used to correct the peak areas for ^{188}Au γ rays. At low energies adjustments were also made for absorption at different angles by the beam stop and detector absorbers. A similar procedure was followed in the ^{186}Au analysis, using a known $E2$ transition (322.9 keV, $\frac{17}{2} \rightarrow \frac{13}{2}$) in ^{185}Au [1].

The resulting intensities were then fitted to the usual distribution

$$W(\theta) = A_0 + A_2 Q_2 P_2(\cos\theta) + A_4 Q_4 P_4(\cos\theta). \quad (1)$$

The Q_2 and Q_4 factors, which are angular attenuation coefficients obtained from the detector crystal geometry, were determined to be 0.97 and 0.90, respectively, with some small variations as a function of γ-ray energy and detector.

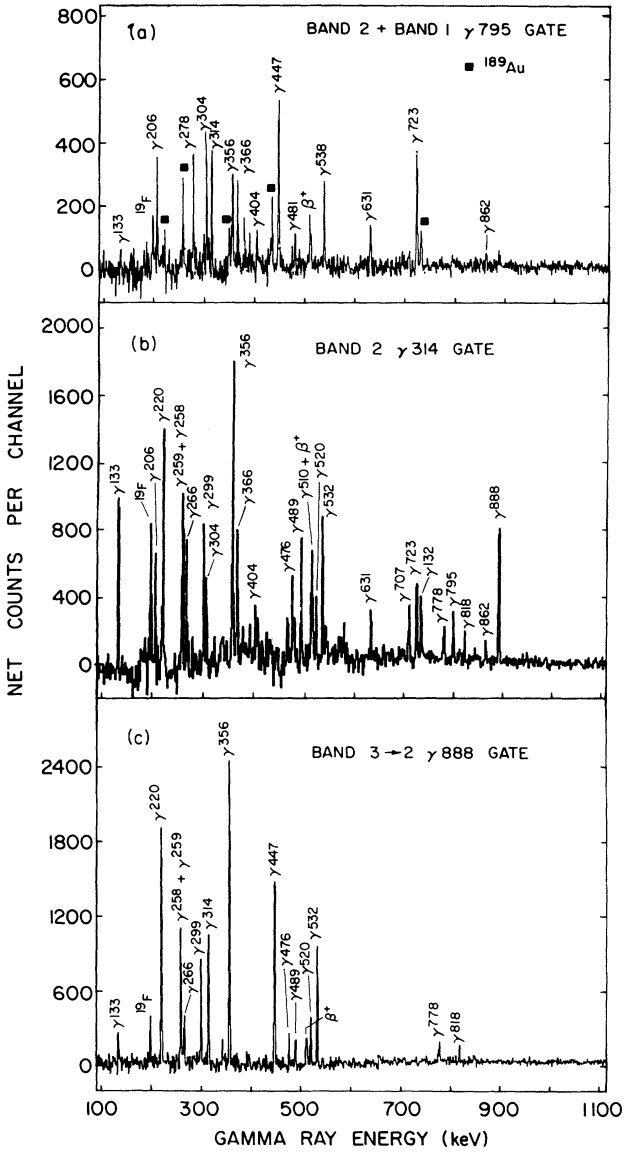

FIG. 3. Selected ^{188}Au background-subtracted coincidence spectra, gated on the (a) 795-, (b) 314-, and (c) 888-keV transitions. Peaks marked by solid squares in the top panel are known contaminants in ^{189}Au.

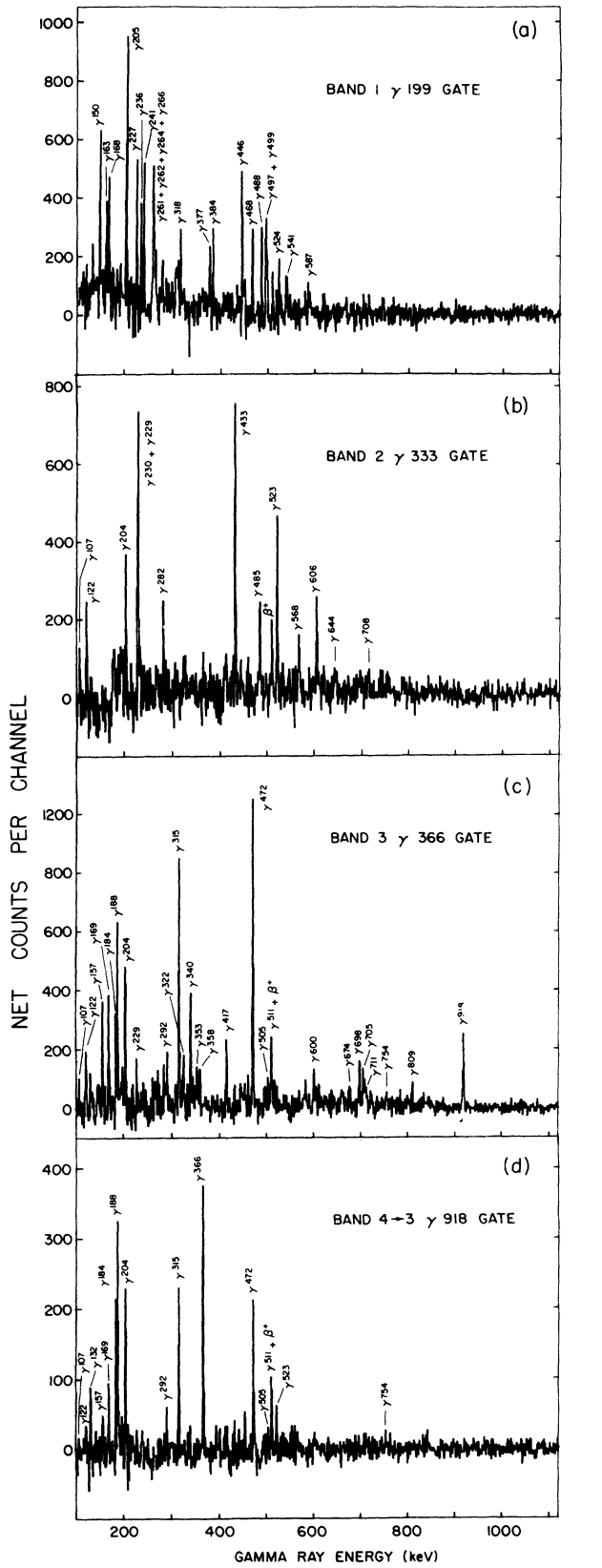

FIG. 4. Selected ^{186}Au background-subtracted coincidence spectra, gated on the (a) 199-, (b) 333-, (c) 366-, and (d) 918-keV transitions.

Illustrative angular distributions are shown in Fig. 5 (^{188}Au) and Fig. 6 (^{186}Au). Tables I and II contain the extracted A_2/A_0 and A_4/A_0 coefficients for ^{188}Au and ^{186}Au, respectively. γ-ray intensities are taken from the A_0 coefficients unless otherwise indicated. For the large majority of reliable cases the angular distribution terms are consistent with either stretched $L = 2$ ($\Delta I = 2$) or mixed $L = 1, 2$ multipolarity. Without information such as abnormal hindrance factors to suggest otherwise, those two options have been taken to indicate transitions having $E2$ and $M1/E2$ character, respectively. Especially for intraband deexcitations following (HI, xn) reactions, it is reasonable to infer a spin change $I \rightarrow I - 1$ for the latter type of transition. In a few cases it was possible to extract $M1/E2$ mixing ratios; the resulting values are small ($|\delta| \leq 0.35$) and are thus unlikely

TABLE I. Energies, relative intensities, angular distribution coefficients and assignments of γ-ray transitions in ^{188}Au.

E_γ [a] (keV)	Band	Relative I_γ [b]	A_2/A_0	A_4/A_0	Assignment $J_i^\pi \rightarrow J_f^\pi$	Multipolarity
133.1	2	11.8±1.2	−0.30±0.03	0.01±0.14	$13^- \rightarrow 12^-$	M1+E2
158.8	1	4.4±1.1	−0.41±0.11	0.04±0.12	$19^- \rightarrow 18^-$	M1+E2
204	2		−0.15±0.03	0.03±0.14	$(20^- \rightarrow 19^-)$	
205.6	1	10.6±1.0			$21^- \rightarrow 20^-$	
220.2	3	29.5±1.9	−0.15±0.03	0.06±0.14	$16^+ \rightarrow 15^+$	M1+E2
257.9	3	4±2[c]			$22^+ \rightarrow 21^+$	
258.4	3	3±1[c]	−0.20±0.05	−0.10±0.15	$24^+ \rightarrow 23^+$	
259.3	3	22.4±2.1	0.02±0.02	−0.04±0.12	$18^+ \rightarrow 17^+$	M1+E2
265.8	3	19±2[c]	0.22±0.02	−0.07±0.12	$17^+ \rightarrow 15^+$	E2
277.8	2	3.6±0.5	−0.38±0.06	0.20±0.18	$18^- \rightarrow 17^-$	M1+E2
299.4	3	27.1±1.7	0.06±0.02	0.00±0.12	$18^+ \rightarrow 17^+$	M1+E2
304.0	1	11.7±1.1	−0.06±0.04	0.06±0.14	$20^- \rightarrow 19^-$	M1+E2
314.3	2	55.2±2.2	−0.05±0.01	0.01±0.11	$12^- \rightarrow 11^-$	M1+E2
356.3	2	76.8±2.3	−0.02±0.01	0.03±0.12	$14^- \rightarrow 13^-$	M1+E2
365.4	2	19±3[c]	−0.07±0.07	0.07±0.18	$16^- \rightarrow 15^-$	
366.4	2	14±2[c]			$15^- \rightarrow 14^-$	
404.0	1	6±2			$22^- \rightarrow 21^-$	
422.3	3 → 2	7.3±1.1	−0.22±0.06	0.20±0.17	$17^+ \rightarrow 16^-$	E1
426.5	2	3.3±0.7	−0.36±0.11	0.11±0.21	$19^- \rightarrow 18^-$	M1+E2
429.4	2	4.7±0.7	−0.35±0.07	0.12±0.18	$17^- \rightarrow 16^-$	M1+E2
447.3	2	≡ 100	0.37±0.01	−0.07±0.11	$13^- \rightarrow 11^-$	E2
476.3	3	16.0±1.52	0.18±0.03	0.01±0.14	$19^+ \rightarrow 18^+$	M1+E2
480.9	2	5.9±0.9	0.46±0.07	−0.16±0.19		
489.4	2	12.7±1.8	0.37±0.06	−0.10±0.14	$14^- \rightarrow 12^-$	E2
509.5	1	5±2[c]			$21^- \rightarrow 19^-$	
519.9	3	12.4±1.2	−0.08±0.04	0.03±0.14	$(21^+ \rightarrow 20^+)$	M1+E2
532.3	3	35.5±2.2	0.35±0.02	−0.10±0.12	$20^+ \rightarrow 18^+$	E2
538.4	1 → 2	11.8±1.2	0.29±0.05	0.10±0.15	$19^- \rightarrow 17^-$	E2
559.6	3	5.1±0.8	−0.02±0.13	0.12±0.20	$23^+ \rightarrow 22^+$	M1+E2
609.8	1	3.4±0.7	0.37±0.17	0.03±0.25	$22^- \rightarrow 20^-$	E2
630.6	2	17.6±1.6	0.33±0.02	−0.01±0.13	$20^- \rightarrow 18^-$	E2
693.7	2	5±2[c]			$(21^-) \rightarrow 19^-$	
704.4	2	4.4±0.9	0.76±0.13	0.07±0.15	$19^- \rightarrow 17^-$	E2
707.2	2	18.3±1.7	0.50±0.03	−0.04±0.14	$18^- \rightarrow 16^-$	E2
722.7	2	39.7±2.4	0.40±0.02	−0.10±0.12	$15^- \rightarrow 13^-$	E2
731.8	2	29±3[c]	0.41±0.06	0.08±0.06	$16^- \rightarrow 14^-$	E2
777.7	3	13.4±1.3	0.34±0.07	−0.04±0.15	$22^+ \rightarrow 20^+$	
794.9	2	21±3[c]			$17^- \rightarrow 15^-$	E2
795	1	2±1[c]	0.40±0.03	−0.05±0.13	$(23^-) \rightarrow 21^-$	
809.2	1 → 2	7.0±1.1	0.30±0.09	0.16±0.19	$18^- \rightarrow 16^-$	E2
818.2	3	9.1±1.2	0.29±0.04	0.00±0.14	$24^+ \rightarrow 22^+$	E2
861.7	2	4.9±1.0	0.20±0.11	0.04±0.13	$? \rightarrow 20^-$	
887.9	3 → 2	65.2±3.3	−0.21±0.01	0.11±0.11	$15^+ \rightarrow 14^-$	E1
940	3				$((26^+) \rightarrow 24^+)$	

[a] Uncertainty of 0.2–0.5 keV, depending on γ-ray intensity.

[b] Normalized to that of the 447.3 keV $13^- \rightarrow 11^-$ transition. When not given $I_\gamma < 3$.

[c] Intensity determined from γ-γ coincidence analysis.

TABLE II. Energies, relative intensities, angular distribution coefficients and assignments of γ-ray transitions in ^{186}Au.

E_γ [a] (keV)	Band	Relative I_γ [b]	A_2/A_0	A_4/A_0	Assignment $J_i^\pi \rightarrow J_f^\pi$	Multipolarity
57	(3 → 2)	(49±10)[c]			$(11^- \rightarrow 10^-)$	
99	1				$(10^+) \rightarrow (9^+)$	
106.8	2	121±7	−0.43±0.07	−0.09±0.07	$8^- \rightarrow 7^-$	M1+E2
117.3	1	44±10[d]			$11^{(+)} \rightarrow (10^+)$	
122.1	2	101±5	−0.44±0.06	0.06±0.06	$9^- \rightarrow 8^-$	M1+E2
131.5	e	15±3[d]			e	
149.5	1	73±4[d]	−0.42±0.05	0.11±0.05	$12^{(+)} \rightarrow 11^{(+)}$	M1+E2
156.5	3	34±3	−0.23±0.09	0.09±0.10	13^-12^-	M1+E2
162.6	1 → 2	75±8[d]	} −0.28±0.02	0.04±0.03	$11^{(+)} \rightarrow 10^{(+)}$	
163.4	2	45±5[d]			$11^- \rightarrow 10^-$	
168.1	1	82±5[d]	−0.14±0.09	0.06±0.06	$13^{(+)} \rightarrow 12^+$	M1+E2
169.4	2	189±7	−0.64±0.03	0.17±0.03	$10^- \rightarrow 9^-$	M1+E2
184.0	e	34±3[d]	0.02±0.08	−0.10±0.10	e	
188.1	4	60±3[d]	0.52±0.04	−0.06±0.05	$(17^+ \rightarrow 15^+)$	(E2)
199.3	1	55±4	−0.43±0.08	−0.06±0.15	$14^{(+)} \rightarrow 13^{(+)}$	M1+E2
203.5	2	48±7	−0.53±0.06	0.15±0.09	$13^- \rightarrow 12^-$	M1+E2
204.4	4	56±5[d]	} −0.26±0.03	−0.06±0.04	$(18^+) \rightarrow (17^+)$	
204.7	1	51±4[d]			$15^{(+)} \rightarrow 14^{(+)}$	
226.9	1	31±2	−0.59±0.06	0.04±0.08	$17^{(+)} \rightarrow 16^{(+)}$	M1+E2
228.5	2	50±5[d]			$9^- \rightarrow 7^-$	E2
229.8	2	80±3	−0.55±0.02	0.01±0.03	$12^- \rightarrow 11^-$	M1+E2
235.9	1	26±4[d]			$19^{(+)} \rightarrow 18^{(+)}$	
241.1	1	33±3[d]	} −0.54±0.03	0.10±0.04	$16^{(+)} \rightarrow 15^{(+)}$	
241.6	2	36±3[d]			$15^- \rightarrow 14^-$	
250	4				$((22^+) \rightarrow (21^+))$	
261.1	1	20±3[d]			$21^{(+)} \rightarrow 20^{(+)}$	
261.5	1	29±4[d]			$18^{(+)} \rightarrow 17^{(+)}$	
263.5	1	24±3[d]			$20^{(+)} \rightarrow 19^{(+)}$	
265.9	1	35±7[d]			$12^{(+)} \rightarrow (10^+)$	
272.1	e	15±3[d]			e	
279.2	2	16±3[d]			$17^- \rightarrow 16^-$	
279.6	1	20±3[d]			$22^{(+)} \rightarrow 21^{(+)}$	
281.5	2	41±2	−0.53±0.04	0.08±0.06	$14^- \rightarrow 13^-$	M1+E2
291.5	2	98±4[d]	0.40±0.02	0.02±0.04	$10^- \rightarrow 8^-$	E2
307.0	1	17±4[d]			$23^{(+)} \rightarrow 22^{(+)}$	
315.4	3	179±14[d]			$12^- \rightarrow 11^-$	M1+E2
317.6	1	65±5[d]	0.47±0.07	−0.31±0.09	$13^{(+)} \rightarrow 11^{(+)}$	E2
320.2	2	9±2[d]			$19^- \rightarrow 18^-$	
322.4	3	16±3[d]			$18^- \rightarrow 17^-$	
326.7	2	21±3[d]			$16^- \rightarrow 15^-$	
332.8	2	≡100	0.33±0.02	−0.04±0.03	$11^- \rightarrow 9^-$	E2
339.7	3	32±3	−0.26±0.06	0.25±0.11	$15^- \rightarrow 14^-$	M1+E2
352.5	3	21±3[d]			$17^- \rightarrow 16^-$	
358.3	3	29±4[d]			$16^- \rightarrow 15^-$	
364.4	2	11±2[d]			$18^- \rightarrow 17^-$	
366.2	3	144±4[d]	} 0.09±0.03	−0.02±0.04	$14^- \rightarrow 13^-$	M1+E2
367.3	1	59±7[d]			$14^+ \rightarrow 12^+$	E2
377.1	e				e	
384.3	1 → 2	91±3	−0.23±0.03	0.02±0.04	$(10^+ \rightarrow 9^-)$	E1
388.6	2	8±2[d]			$20^- \rightarrow 19^-$	
392.9	2	107±4	0.26±0.03	−0.08±0.04	$12^- \rightarrow 10^-$	E2
404.0	1	57±3	0.35±0.10	0.05±0.07	$15^{(+)} \rightarrow 13^{(+)}$	E2
433.3	2	111±4	0.27±0.05	0.08±0.05	$13^- \rightarrow 11^-$	E2
445.7	1	53±3	0.31±0.05	−0.02±0.05	$16^{(+)} \rightarrow 14^{(+)}$	E2
455.1	e	23±2[d]	−0.28±0.04	−0.11±0.04	e	M1+E2
468.0	1	52±4	0.28±0.05	0.01±0.07	$17^{(+)} \rightarrow 15^{(+)}$	E2

TABLE II. (*Continued*).

E_γ [a] (keV)	Band	Relative I_γ [b]	A_2/A_0	A_4/A_0	Assignment $J_i^\pi \rightarrow J_f^\pi$	Multipolarity
471.8	3	136±8[d]			$13^- \rightarrow 11^-$	
485.2	2	65±3	0.32±0.03	−0.03±0.06	$14^- \rightarrow 12^-$	E2
488.1	1	45±3[d]			$18^{(+)} \rightarrow 16^{(+)}$	
497.2	1	50±3[d]			$19^{(+)} \rightarrow 17^{(+)}$	
499.4	1	42±3[d]			$20^{(+)} \rightarrow 18^{(+)}$	
504.6	4	20±3[d]	−0.19±0.13	0.27±0.16	$(21^+) \rightarrow (20^+)$	(M1+E2)
510.9	4	88±30[d]			$(20^+) \rightarrow (18^+)$	
522.6	3	61±4[d]	} 0.42±0.04	0.05±0.06	$14^- \rightarrow 12^-$	
523.4	2	90±5[d]			$15^- \rightarrow 13^-$	E2
524.3	1	36±3[d]			$21^{(+)} \rightarrow 19^{(+)}$	
540.8	1	37±3[d]			$22^{(+)} \rightarrow 20^{(+)}$	
568.4	2	50±3	0.34±0.09	0.15±0.10	$16^- \rightarrow 14^-$	E2
586.5	1	17±2[d]			$23^{(+)} \rightarrow 21^{(+)}$	
600.6	e	29±3[d]			e	
606.0	2	67±4[d]			$17^- \rightarrow 15^-$	
610.1	e	23±2[d]			e	
643.8	2	41±3[d]			$18^- \rightarrow 16^-$	
674.2	3	33±3[d]			$18^- \rightarrow 16^-$	
684.6	2	40±3[d]			$19^- \rightarrow 17^-$	
698.1	3	50±5	0.33±0.19	0.07±0.17	$16^- \rightarrow 14^-$	E2
705.6	3	79±3	0.32±0.06	−0.11±0.07	$15^- \rightarrow 13^-$	E2
708.3	2	33±3[d]			$20^- \rightarrow 18^-$	
710.5	3	41±3[d]	0.51±0.21	−0.29±0.23	$17^- \rightarrow 15^-$	E2
741	2				$((21^-) \rightarrow 19^-)$	
754.4	4	39±3[d]			$(22^+) \rightarrow (20^+)$	
757	2				$((22^-) \rightarrow 20^-)$	
808.9	e	31±3[d]			e	
918.0	4 → 3	82±4	−0.31±0.05	0.04±0.08	$15^+ \rightarrow 14^-$	E1

[a] Uncertainty of 0.2–0.5 keV, depending on γ-ray intensity.

[b] Normalized to that of the 332.8 keV $11^- \rightarrow 9^-$ transition. When not given $I_\gamma < 8$.

[c] Based on intensity feeding 11^- isomer.

[d] Intensity determined from γ-γ coincidence analysis.

[e] Not placed in level scheme.

to have a significant effect on further analysis such as $B(M1; I \rightarrow I-1)/B(E2; I \rightarrow I-2)$ ratios (see Sec. IV C) and total intensity derivations. A few γ rays exhibit angular coefficients consistent with pure $L = 1$ transitions, taken to imply $E1$ character.

C. γ-γ lifetime measurements

Knowing that isomers in the nanosecond range have been identified in the neighboring odd-A Au isotopes [22–24], we performed an additional γ-γ-t experiment in parallel with the angular distribution measurements. In addition to the five Ge coaxial detectors already mentioned, a low-energy photon spectrometer (LEPS) was placed at a backward angle 7 cm from the target. The LEPS was a planar Ge detector with an active volume of 15 cm^3 and a resolution of approximately 0.9 keV at 122 keV. Standard nanosecond timing techniques were used to acquire coincidences between any Ge coaxial detector and the LEPS as γ_1-γ_2-t events, gated by the multiplicity filter. Since there were insufficient statistics to warrant a complete analysis extracting time spectra corresponding to narrow windows on both the Ge and the LEPS γ-ray energies, the data tapes were subsequently sorted in the following two ways: (1) Narrow γ-ray energy gates were set on peaks of interest in the coaxial Ge projection, and time spectra projected out for an open LEPS gate ($\approx$ 90–600 keV). (2) Conversely, narrow gates were set on γ-ray peaks in the LEPS projection, and time spectra projected out for an open coaxial Ge gate. In both cases background events were subtracted using gates set nearby the peaks of interest.

The time spectra generated in such a generous manner are naturally dominated by a large peak due to prompt γ-γ events, with a width in this case of approximately 12 ns FWHM. However, by gating on sequences of γ-ray peaks above and below a level suspected of isomeric behavior, using both methods as outlined above, one is able to extract the lifetime of such a level.

Only one isomeric level in the $10 \leq \tau \leq 200$ ns range was found during the lifetime analysis, in ^{186}Au. Figure 7 contains examples of time spectra gated by (a) γ-

ray peaks in the coaxial Ge projection corresponding to transition placed in the band *above* the isomer, (b) γ-ray peaks in the LEPS projection for transitions placed in the level scheme *below* the isomer, and (c),(d) γ-ray peaks in the coaxial Ge projection for transitions with no supposed connection to the isomer. The case (a) spectrum in Fig. 7 reveals a long-lived decay on the "positive" side of the prompt time peak. Based on a number of such spectra a half-life of $T_{1/2} = 39 \pm 4$ ns was extracted for a proposed 11^- state (see Sec. III B 3). The spectrum corresponding to case (b) shows a decay with the same lifetime, while the examples for cases (c) and (d) reveal only prompt events above the level background.

III. LEVEL SCHEMES

The ^{188}Au and ^{186}Au level schemes are shown in Figs. 8 and 9, respectively. Spin and parity assignments are discussed in Secs. III A and III B below, while the quasiparticle structure and subsequent interpretation follow in Sec. IV.

A. ^{188}Au level scheme

Previous work established the ground-state spin of 1^- [25] and the ground-state magnetic moment [26], as well as low-spin levels populated by the decay of ^{188}Hg [27].

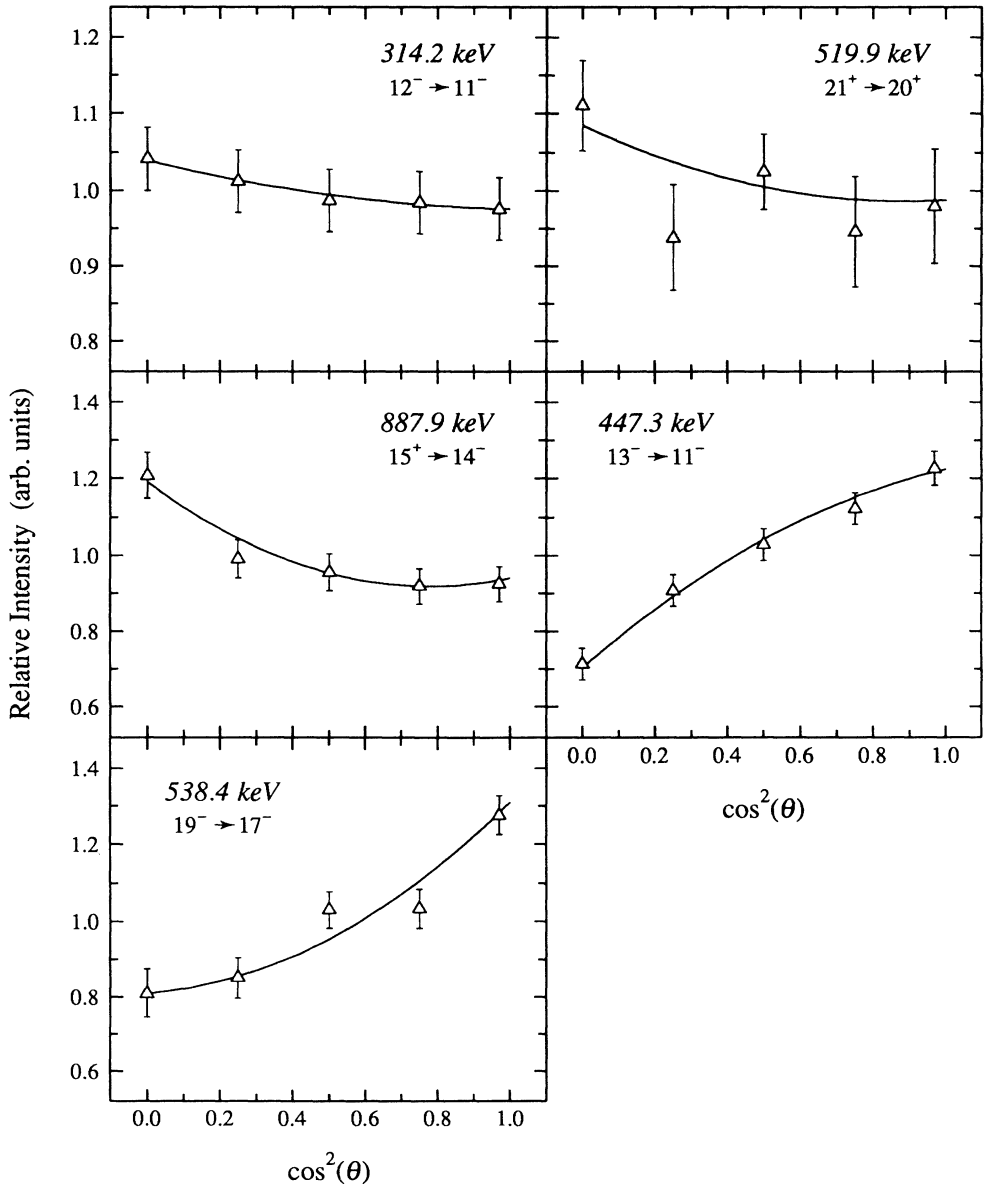

FIG. 5. Selected ^{188}Au γ-ray angular distributions. Solid lines indicate fits to the data. The extracted A_2/A_0 and A_4/A_0 coefficients are listed in Table I.

However, only preliminary in-beam results have been reported elsewhere [28].

1. Band 2

The most intense γ rays observed in the present work belong to a level structure labeled band 2 in Fig. 8, which displays a striking similarity to bands observed in the neighboring odd-odd ^{190,192,194}Au isotopes [17,18]. This sequence of bands for $^{186-192}$Au is shown in Fig. 10. In the ^{192,194}Au cases the 11^- bandhead lifetimes and decays to low-spin levels have been established, while in ^{190}Au an 11^- lifetime has been measured but the decay path has not been discovered. Based on the systematic progression of these bands as a function of neutron number, we have assigned spin and parity 11^- to the ^{188}Au bandhead. We have not been able to determine either a lifetime or a subsequent decay scheme. Presumably the lifetime is greater than the experimental limit of 400 ns, consistent with the millisecond lifetimes measured in the heavier odd-odd Au nuclei [18]. The excitation energy of the 11^- isomer with respect to the ground state is not known (neither is it in ^{190}Au) and for the purposes of this discussion is set to 0 keV. An extrapolation from the ^{192,194}Au level schemes [17] indicates that the 11^- state should lie approximately 400 keV above the ground state.

Two other characteristics of band 2 fit the known sys-

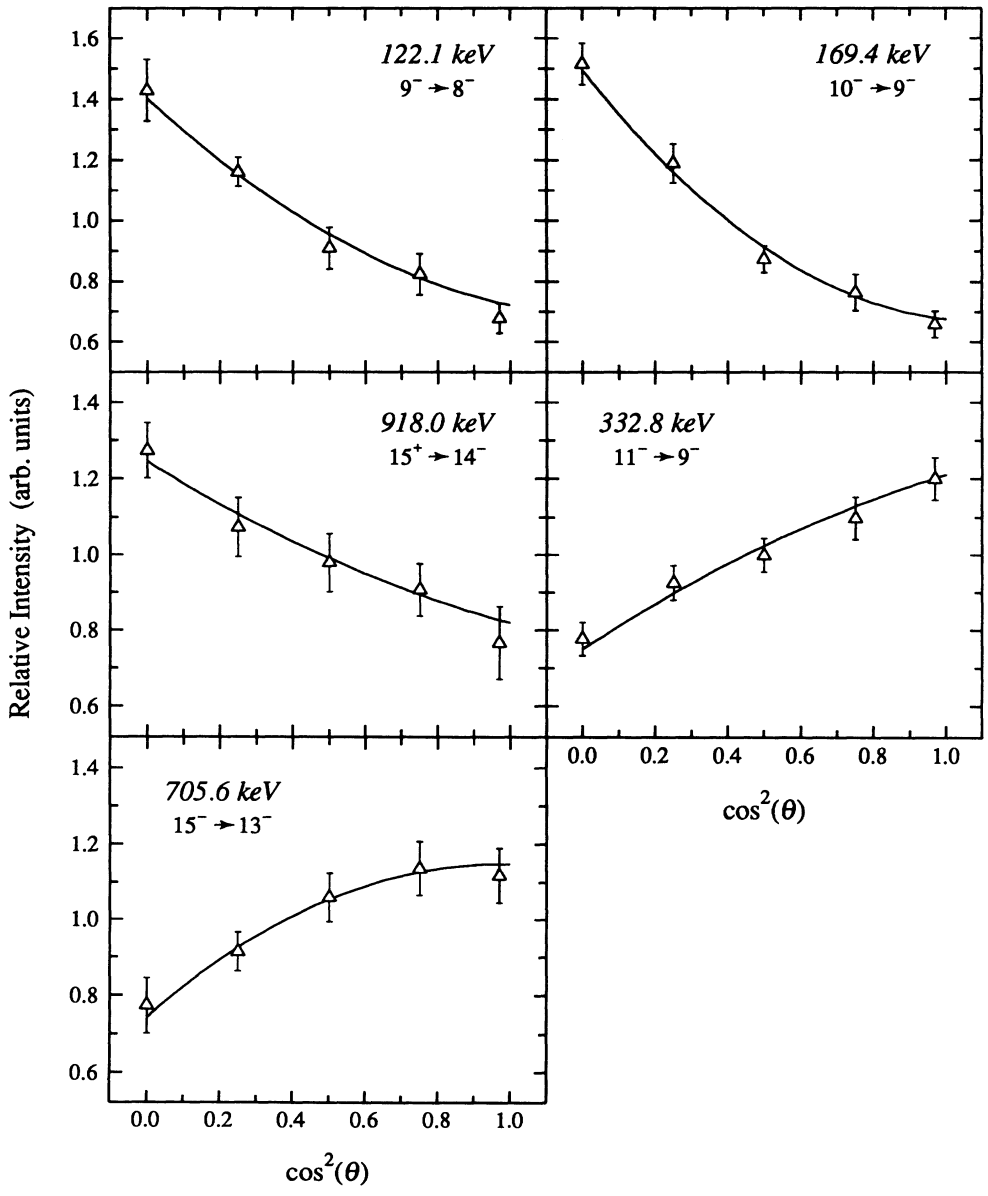

FIG. 6. Selected ^{186}Au γ-ray angular distributions. Solid lines indicate fits to the data. The extracted A_2/A_0 and A_4/A_0 coefficients are listed in Table II.

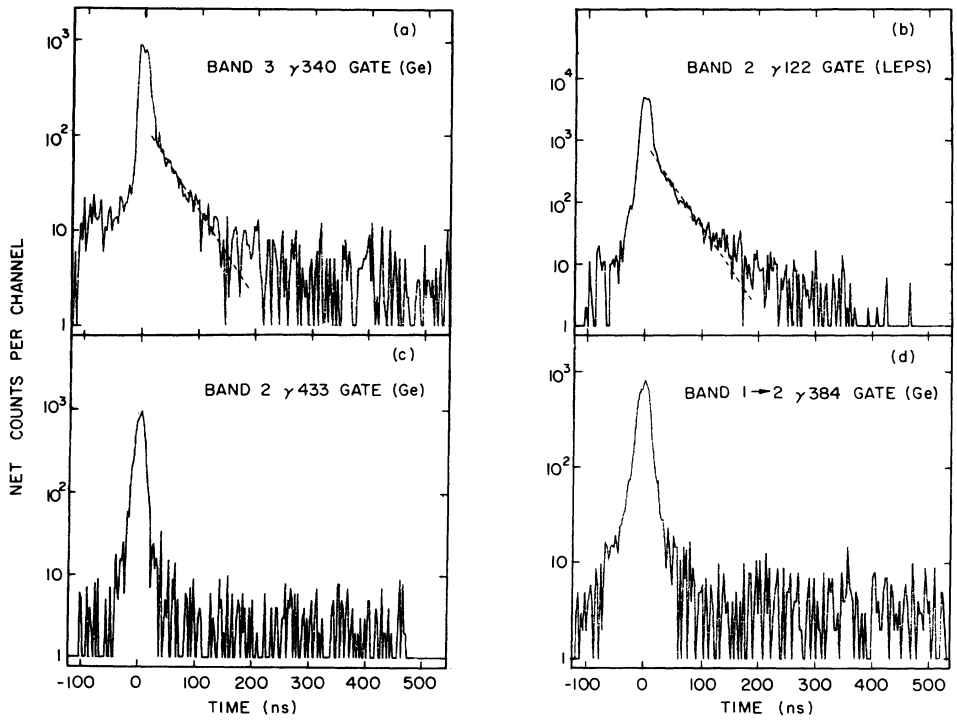

FIG. 7. ^{186}Au time spectra gated by the following transitions: (a) 340 keV (in coaxial Ge detector), placed above the isomer in the level scheme; (b) 122 keV (in LEPS detector), below the isomer; (c) 433 keV (in coaxial Ge detector), bypassing the isomer; and (d) 384 keV (in coaxial Ge detector), connecting bands 1 and 2. The dashed lines in panels (a) and (b) correspond to $T_{1/2} = 39.5$ ns.

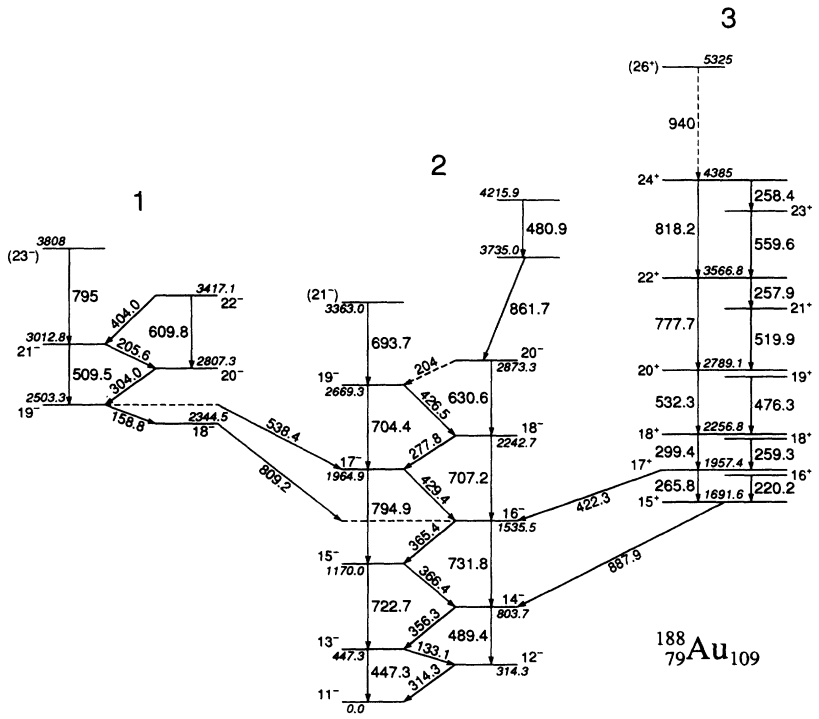

FIG. 8. Level scheme for ^{188}Au. Spins and parities are based upon the assumption that the lowest observed level has $I^{\pi} = 11^{-}$, as discussed in the text and illustrated in Fig. 10. The ground state has $I = 1$ [25] but no decay from the proposed 11^{-} state to the ground state can be assigned from the present work. Levels are labeled with their excitation energy in keV relative to the 11^{-} bandhead.

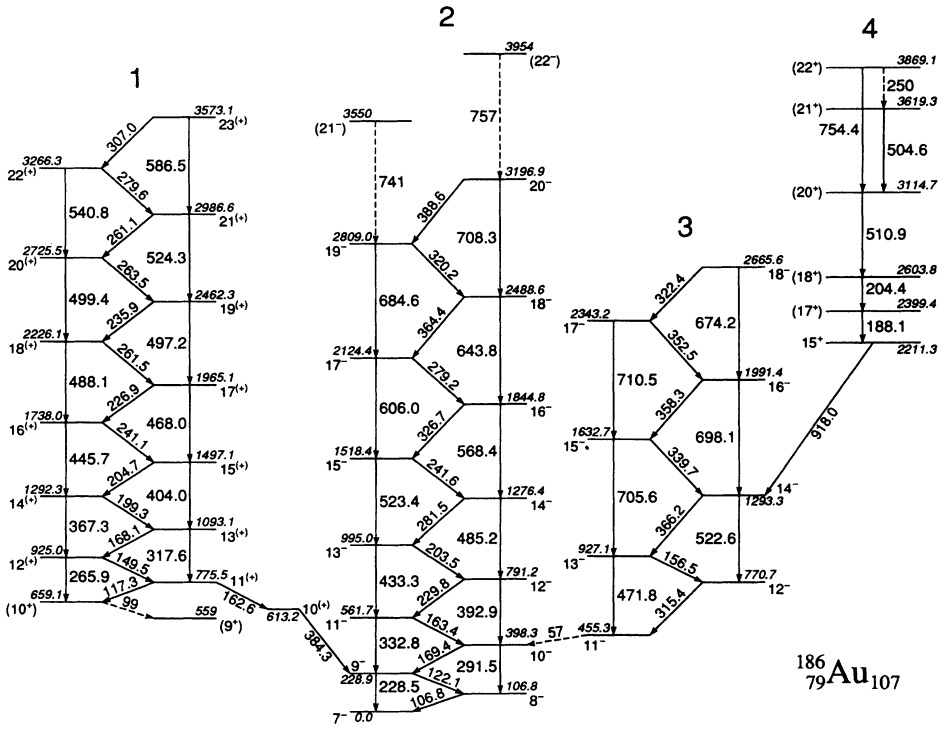

FIG. 9. Level scheme for ^{186}Au. Spins and parities are based upon the assumption that the lowest observed level in band 3 has $I^{\pi} = 11^{-}$, as discussed in the text and illustrated in Fig. 10. The ground state has $I = 3$ [25] but no decay either from the proposed 11^{-} or 7^{-} state to the ground state can be assigned from the present work. States are labeled with their excitation energy in keV relative to the 7^{-} level.

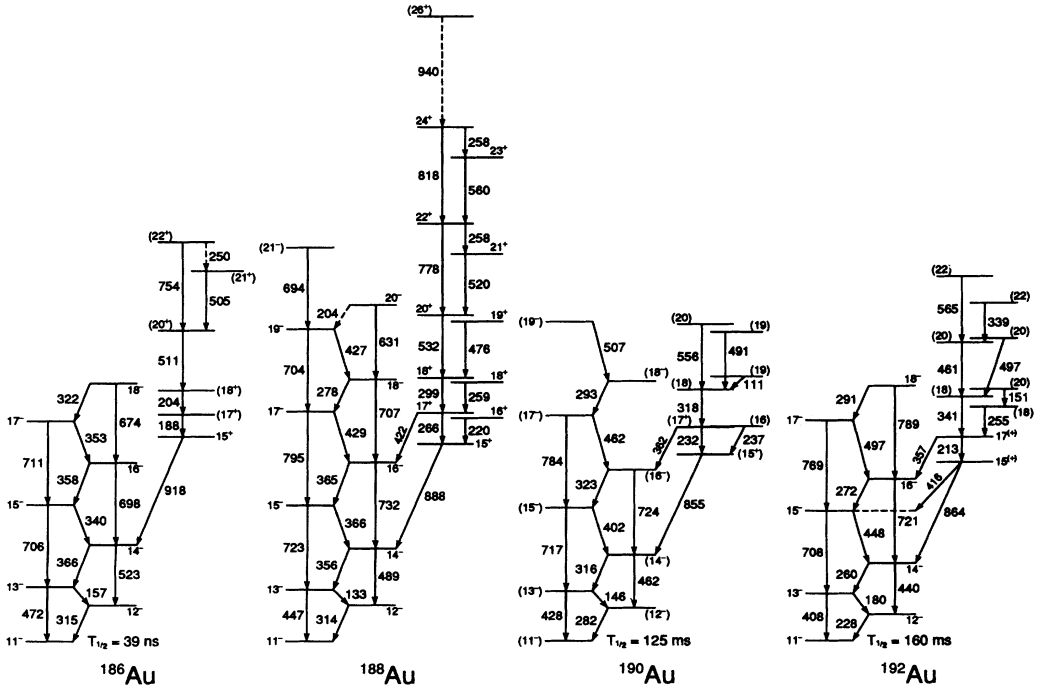

FIG. 10. Systematics of 11^{-} and 15^{+} band structures in odd-odd $^{186-192}$Au, taken from the present work and Ref. [17].

tematic behavior of the odd-odd Au isotopes. First, the $\Delta I = 2$ energy spacings, and also the energy staggering between the odd and even spin members, vary smoothly from $A = 194$ to $A = 186$ (see Sec. IV A 4, as well as Fig. 10). Second, as shown in Fig. 10, the presence of bands built on $I = 15$ states lying 800–900 keV above the 14^- levels is a distinctive feature in these nuclei. Therefore, although the spins and parities of the levels in ^{188}Au band 2 cannot be directly established, the evidence is clearly in favor of the proposed 11^- bandhead assignment.

The 480.9- and 861.7-keV γ rays feed the 20^- state but no clear additional level structure could be associated with them. The corresponding intensities are within the quoted uncertainties of each other and the order of the two transitions is not clear.

2. Band 3

The energy levels grouped into band 3 of Fig. 8 form a more irregular structure based on a proposed 15^+ state. This assignment follows two arguments. Angular distributions of the 887.9- and 422.3-keV γ rays are both consistent with pure dipole $\Delta I = 1$ (most likely $E1$) transitions. Second, as discussed in the preceding section, the clear presence of 11^- and 15^+ bandheads is a distinctive and systematic feature in these odd-odd Au nuclei.

γ rays shown in level structure 3 can be grouped into two subsets, based on their angular distributions. The 265.8-keV γ ray falls into a group having $\Delta I = 2$ (assumed to be $E2$) characteristics, consistent with the 887.9 and 422.3 keV transitions both being assigned as dipole. The remaining γ rays in clear concidence with each other, placed above the 15^+ level, are in the $E2$ category as well, with the exception of the 299.4-keV transition. It falls into a second group, those having $\Delta I = 1$ $M1/E2$ characteristics. The transitions placed on the right-hand side of band 3 in the level scheme are all in that same category.

Therefore band 3 actually appears to be made up of two structures, one of which is comprised of the 15^+, 17^+, and possibly (16^+) levels. The second structure resembles the coupled band 1, but with a more pronounced energy staggering between odd and even spin levels. In each of the odd-odd Au isotopes, the signature splitting in this structure changes completely between $I = 17$ and 18. This feature is not understood, although a possible explanation is discussed in Sec. IV B 3.

3. Band 1

This structure feeds into the 11^- band at spins 16^- and 17^-. The $E2$ character of the 538.4- and 809.2-keV transitions determines the spins and parities of the two lowest levels in band 1 as shown. Due to impurities and low intensities, clear angular distributions are only possible for the 158.8-, 304.0-, and 609.8-keV γ rays. The spin and parity of the 21^- member assumes $M1/E2$ $\Delta I = 1$ character for the 205.6 and 404.0 keV γ rays, consistent with a parallel 609.8-keV $E2$ transition.

B. ^{186}Au Level Scheme

The low-spin levels of ^{186}Au are known from decay work [29] and an atomic-beam measurement of the ground-state spin [25]. Thus the ground state is known to have $I = 3$ [25], and the parity is assumed to be negative based on ground-state properties of adjacent odd-A nuclei (see Sec. IV B). Some preliminary in-beam data have been reported by Porquet [30], comprising the very low-spin portion of band 2 and some transitions included in band 3 of the present level scheme shown in Fig. 9. Although no connection was observed between the two level structures in that previous study, the data presented here indicate that band 3 does feed into band 2. In addition, two new level structures (1 and 4) have been placed in the decay scheme as outlined below.

1. Band 3

Band 3 in ^{186}Au displays the same characteristic energy spacings as the 11^- bands in odd-odd $^{188-194}$Au (cf. Fig. 10). Following the same arguments as in Sec. III A, we have assigned the bandhead spin and parity 11^-. The isomer search (Sec. II C) resulted in a measured half-life of $T_{1/2} = 39 \pm 4$ ns.

2. Band 4

The angular distribution of the 918.0-keV γ ray indicates a dipole transition, suggesting decay from a 15^+ state. Band 4 shows the same behavior as does band 3 in ^{186}Au, following the systematics of the heavier odd-odd Au isotopes. A similar change in structure at spin 18 is observed, although in this case only the beginning of a band with pronounced odd-even staggering is detected.

3. Band 2

Marking a clear departure from the heavier odd-odd Au nuclei, the yrast structure 2 displays a coupled level scheme with smoothly increasing energy spacing and a consistently small odd-even staggering. As seen in Fig. 4, the γ-γ spectrum gated by the ^{186}Au 366.2-keV transition, placed above the 11^- isomer, clearly shows a number of transitions placed in band 2. The manner in which the isomer feeds into the lower band could not be definitely established. However, based on LEPS spectra gated on coaxial Ge peaks known to be above the isomeric level (an example of which is shown in Fig. 11), a 57-keV transition is proposed as the most likely link between the two band structures. The γ-γ spectra gated on band 3 transitions show the absence of band 2 γ rays placed above the level assigned as 10^- (see below) in Fig. 9. This is consistent with an abrupt drop in γ-ray intensity above that same level.

Since an $E2$ 57-keV γ ray is incompatible with the measured 11^- lifetime, and a $\Delta I = 0$ transition is inconsistent with the observed lack of $\Delta I = 1$ transitions to lower-lying levels in band 2, we have assumed the 11^- isomeric state decays to a 10^- level in band 2. An alternative would be to assign positive parity to this band,

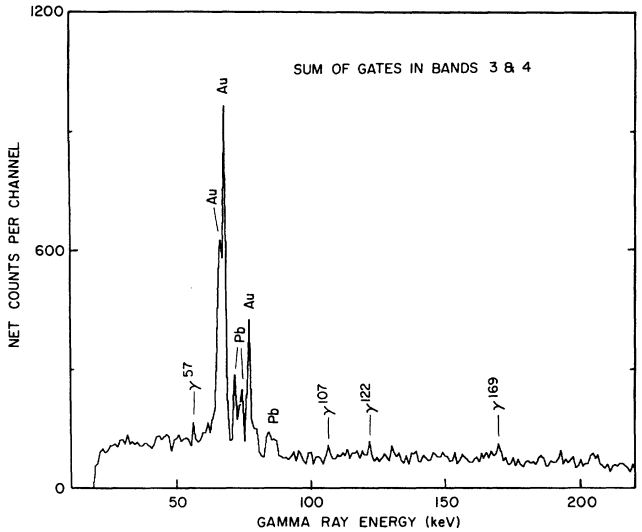

FIG. 11. Sum of LEPS γ-ray spectra gated on the 315-, 472-, 157-, 366-, 706-, and 754-keV transitions in bands 3 and 4 of ^{186}Au, subtracted for background. γ rays assigned to ^{186}Au are marked by energy, while Au and Pb denote x-rays. It is proposed that a 57-keV transition is the most likely link between bands 2 and 3.

making the 57-keV γ ray an $E1$ transition. But as discussed in Sec. IV A, a comparison with neighboring nuclei favors negative parity. Band 2 is thus based on a 7^- "bandhead," with no clear transitions to the known 3^- ground state, although it is possible that these two states are members of the same rotational band. The four $\Delta I = 1$ transitions between the $I = 7$ and 3 levels would have energies less than 100 keV, and are not observed due to the presence of strong x-ray peaks, low detector efficiency, and/or large internal conversion.

Angular distributions could not be extracted for the γ rays placed above the 16^- level. However, the presence of interlocking high- and low-energy transitions plus the regular behavior of the energy levels are strong arguments in support of the proposed spin and parity assignments.

4. Band 1

This structure becomes the yrast band above spin 14. At lower spins it can be followed down to a proposed (9^+) state which, as in the case of band 2, is probably not the true bandhead. A direct link between bands 1 and 2 was not observed; the strongest connection, shown in Fig. 9, is via the 162.6 + 384.3 keV pathway. The A_2 and A_4 values for the 384.3-keV line have rather small uncertainties and are compatible with a pure $L = 1$ transition. This leads us to prefer an $E1$ multipolarity for this transition, although we cannot exclude the possibility of an unmixed $M1$ transition. The 162.6-keV γ ray is part of an unresolved doublet. The other member of that doublet, the 163.4-keV $11^- \rightarrow 10^-$ transition, probably has an A_2 of -0.55 ± 0.10, by comparison with the angular distribution coefficients of other $M1/E2$ γ rays in band 2. Based on the intensity distribution of the doublet and the composite A_2 of -0.28 ± 0.02, we can estimate a 162.6-keV A_2 of -0.12 ± 0.09. Although not exclusive of a pure dipole assignment, this value is characteristic of an $M1/E2$ $\Delta I = 1$ transition. A spin of 10 for the intermediate level between bands 1 and 2 is therefore favored, while a positive-parity assignment can only be suggested. As discussed in Secs. IV A 3 and IV A4, the most likely configurations of low-lying Nilsson orbitals for this band have positive parity. Note that the ordering of the 162.6- and 384.3-keV transitions is unclear. Since the 384.3-keV γ ray has the larger intensity of the two, it has been placed below the 162.6-keV transition.

Band 1 also decays down to $I = 10$ (and possibly $I = 9$) with no observed transitions feeding out. In addition, there is considerably more intensity feeding the proposed $10_2^{(+)}$ state than there is decaying from it. The missing intensity may well be carried away by a number of low-energy transitions which remain unobserved for reasons similar to those discussed with respect to band 2. The presence of two close-lying 10^+ states would signify the existence of another positive-parity sequence of states, which due to mixing could lead to further fragmentation of the γ-ray intensity. As discussed in Sec. IV A, there is good evidence for such a possibility occurring in ^{186}Au.

IV. DISCUSSION

A. Prolate bands

1. Single-particle states

The ground-state angular momenta of the light gold nuclei have been determined in atomic-beam magnetic-resonance experiments. The ground-state nuclear spins of ^{186}Au and ^{188}Au were measured by Ekström *et al.* [25] to be $I = 3$ and 1, respectively. This spin value for ^{188}Au is the same as that of the ground states of heavier odd-odd gold nuclei ($A = 190$ [31,32], $A = 192$ [33], and $A = 194$ [33] and is logical in view of the ground spins of the neighboring odd-A nuclei. As discussed by Porquet *et al.* [29], ^{187}Pt has a ground-state spin of $I = \frac{3}{2}$ [34] ($\nu p_{3/2}$) and ^{187}Au and ^{189}Au have $I = \frac{1}{2}$ [25] ($\pi d_{3/2}$). The change in spin of the ground state of ^{186}Au from $I = 1$ to 3 is accompanied by a change in deformation, as deduced from the resonance-ionization mass spectrometry performed by Wallmeroth *et al.* [3]. They measured a large change in the mean square charge radius between ^{187}Au and ^{186}Au, an indication that the ground state of the latter is rather prolate deformed ($\beta \simeq 0.25$ [3]) while the heavier gold nuclei have small oblate deformations. This sudden change agrees with the change in the ground-state configurations of the adjacent odd-A nuclei. The ground state of the odd-N Pt nuclei switches from $I = \frac{3}{2}$ to $\frac{9}{2}$ at $A = 185$, which is thought [29] to be the bandhead of the $\frac{9}{2}$ [624] prolate Nilsson configuration ($\nu i_{13/2}$). Also, the ground state of ^{185}Au is $I = \frac{5}{2}$ (rather than $\frac{1}{2}$ as for the heavier isotopes), which is interpreted [26] as the lowest member of the prolate $\frac{1}{2}$ [541] band ($\pi h_{9/2}$). The information on low-lying configurations in odd-A nuclei in this region is given in Table III. In the odd-A Au nu-

TABLE III. Low-lying quasiparticle configurations observed in odd-A nuclei neighboring ^{186,188}Au. The notations (pro) and (obl) refer to known prolate or oblate configurations, respectively.

Configuration	$^{185}_{79}Au_{106}$ (Ref. [1])	$^{187}_{79}Au_{108}$ (Refs. [6,23])	$^{189}_{79}Au_{110}$ (Refs. [36,37])
Ground state	$\frac{5}{2}^-$ (pro)	$\frac{1}{2}^+$ (obl)	$\frac{1}{2}^+$ (obl)
$\frac{9}{2}^-$ $(\pi h_{9/2})$	8.9 keV (pro)	120.7 keV (pro)	326.5 keV (obl)
$\frac{13}{2}^+$ $(\pi i_{13/2})$	859.8 keV (pro)	1122.0 keV (pro)	1383 keV (obl)
$\frac{11}{2}^-$ $(\pi h_{11/2})$	220.0 keV (pro)	224.6 keV (obl)	248.5 keV (obl)
	$^{185}_{78}Pt_{107}$ (Refs. [9,38,39])	$^{187}_{80}Hg_{107}$ (Refs. [40,41])	
Ground State	$\frac{9}{2}^+$ (pro)	$\frac{3}{2}^-$ (obl)	
$\nu i_{13/2}$ bandhead	0 keV (pro) $\frac{9}{2}$[624]	$x \simeq 85$ keV (obl)[a]	
		$x + 161$ keV (pro)	
$\nu \frac{1}{2}$[521] bandhead	103.2 keV		
$\nu \frac{7}{2}$[503] bandhead	310.4 keV		
$\nu \frac{7}{2}$[514] bandhead	449.9 keV		
	$^{187}_{78}Pt_{109}$ (Refs. [40,42–44])	$^{189}_{80}Hg_{109}$ (Refs. [45,46])	
Ground state	$\frac{3}{2}^-$ (obl)	$\frac{3}{2}^-$ (obl)	
$\nu i_{13/2}$ bandhead	203.2 keV (obl)	95.1 keV (obl)	

[a] From systematics [41] the oblate $\nu i_{13/2}$ bandhead is estimated to lie approximately 85 keV above the ground state. The prolate $\nu i_{13/2}$ bandhead is known to be 161 keV higher [41].

clei, the $\pi h_{9/2}$ excitation is falling rapidly for the lighter nuclei, becoming the ground state for $A = 185$. As suggested by Porquet *et al.* [29], a possible configuration for the prolate ground state of ^{186}Au is thus $\pi h_{9/2} \otimes \nu i_{13/2}$. The low-spin members of the $\frac{1}{2}$[541] band in ^{185}Au are Coriolis mixed, which results in the ground state having $I = \frac{5}{2}$ rather than $\frac{1}{2}$ (strong-coupling limit) or $\frac{9}{2}$ (weak-coupling limit). The ground-state spin of ^{186}Au ($I = 3$) could likewise result from a complicated degree of mixing in the $\pi h_{9/2}$ system and thus would not be a simple vector addition of the valence neutron spin ($\frac{5}{2}$) and proton spin ($\frac{9}{2}$) [29,35].

As discussed in the preceding section, the yrast band (band 2 in the level scheme of Fig. 8) observed in our measurements on ^{188}Au is assigned by analogy to those known previously in the heavier odd-odd isotopes. This band is based on an 11^- level and results from the coupling of the $h_{11/2}$ proton and $i_{13/2}$ neutron states. As seen in Table III, the $\pi h_{11/2}$ structure is regularly around 200 keV above the ground state in the odd-A nuclei, while the oblate $\nu i_{13/2}$ band lies low in energy in odd-N Hg nuclei for $N \geq 107$. No transitions can be proposed from our experiments between the 11^- bandhead and the 1^- ground state in ^{188}Au.

The same slightly oblate $\nu i_{13/2}^{-1} \otimes \pi h_{11/2}^{-1}$ band is proposed to be present and built on an 11^- level in ^{186}Au. (These are hole configurations built on oblate Hg-like cores rather than particle states built on prolate Pt-like cores. Note that we write $\pi \otimes \nu$ configurations for prolate bands and $\nu \otimes \pi$ for oblate.) As shown in the level scheme of Fig. 9, this band 3 is not yrast but decays to the strongly coupled band 2 (which is yrast at low spins). The ground state of ^{186}Au is the prolate $\pi h_{9/2} \otimes \nu i_{13/2}$ coupling [29], and it is logical that the lowest-lying band seen here would be the same configuration (this will be discussed further in the following section). However, the transitions between the "bandhead" observed here ($I = 7$) and the known ground state ($I = 3$) could not be assigned. These are presumably four $\Delta I = 1$ transitions with energies below 80 keV. A comparison of this band 2 with the assigned $\pi h_{9/2} \otimes \nu i_{13/2}$ band in the isotone ^{184}Ir [11] is shown in Fig. 12. The ground state of ^{184}Ir is known to be $I = 5$, and the connection of the yrast band to it is observed [11]. The ground-state spin is different for these two isotones; the Coriolis mixing is presumably not the same, a result of the variation in the proton Fermi surface. Band 2 in ^{186}Au is representative of a slightly smaller deformation, but is otherwise very similar to the assigned $\pi h_{9/2} \otimes \nu i_{13/2}$ band of ^{184}Ir (e.g., in the degree of signature splitting, which will be discussed in the following section).

It is not readily apparent from the data shown in Table III what the quasiparticle composition of band 1 in ^{186}Au might be. It is necessary to consider additivity of one-quasiparticle components in some detail before a proposal can be made for this.

2. *One-quasiparticle Routhians*

In order to deduce the quasiparticle composition of the observed bands, one must consider not only the additivity of bandhead spins from the odd-A to the studied odd-odd

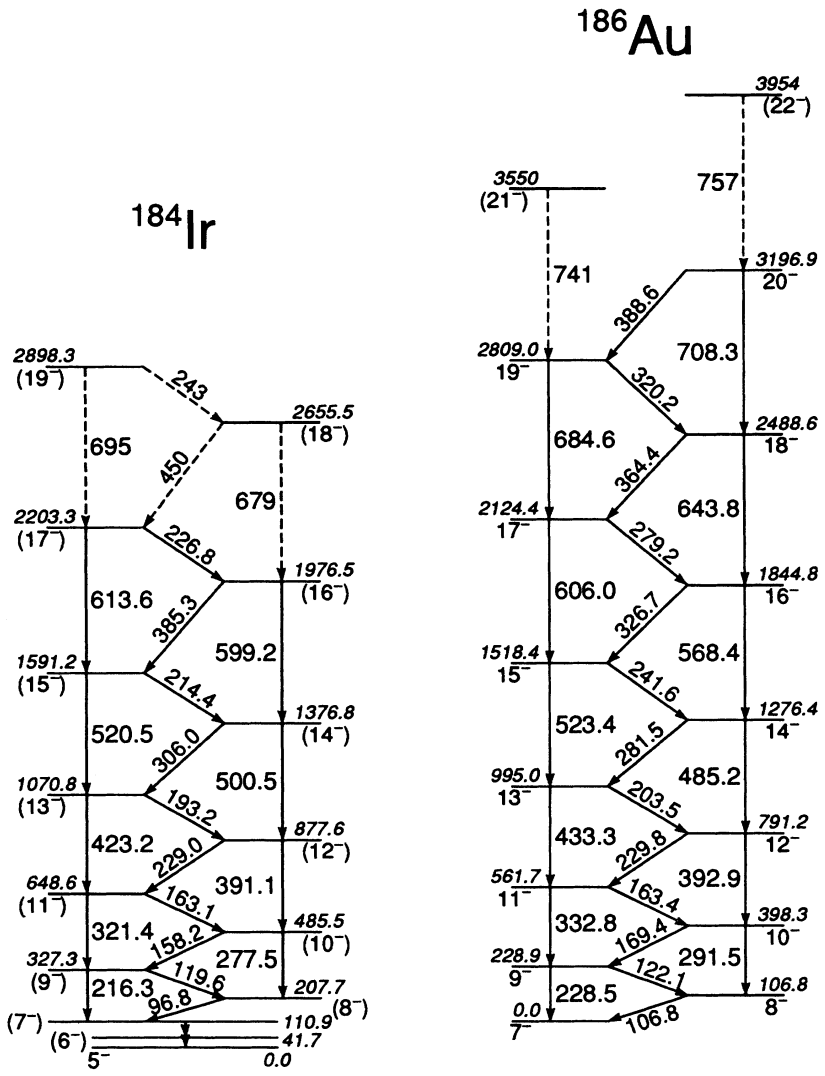

FIG. 12. The prolate $\pi h_{9/2} \otimes \nu i_{13/2}$ bands in ^{184}Ir [11] and ^{186}Au. The excitation energy of the 7^- state in ^{186}Au is unknown (see text).

nucleus but also the additivity at higher rotational frequencies. This can best be accomplished by converting the measured energies and spins to the rotating frame of the nucleus, as outlined by Bengtsson and Frauendorf [47]. The experimental Routhians (energies in the rotating frame) for prolate bands in nuclei adjacent to ^{186}Au, i.e., ^{185}Au [1], ^{187}Au [6], ^{185}Pt [4,9], and ^{187}Hg [10] are shown in Fig. 13 as a function of rotational frequency. The reference parameters, $\mathcal{J}_0$ and $\mathcal{J}_1$, are chosen in a way to be consistent with the calculated trends of deformation and shape softness. For example, the deformation should increase with decreasing N, which gives rise to an increasing $\mathcal{J}_0$. The $\mathcal{J}_1$ values are smoothly varied with N to give constant alignments in two-quasiparticle bands in ^{184}Pt ($N = 106$) and ^{186}Pt (108). At $N = 107$, the $\mathcal{J}_1$ value increases as $\mathcal{J}_0$ and deformation decrease. Only the prolate bands are shown in Fig. 13, since the ground state of ^{186}Au is known to be prolate [3] and it is assumed (see the following discussion) that the dominant bands seen here (bands 1 and 2) are built on prolate shapes. To facilitate discussion of the Routhians at higher frequency, we use letters as labels to denote quasiparticle configurations as defined in Table IV. The Nilsson asymptotic quantum numbers given for the bands are appropriate only at low rotational frequency.

It seems obvious from Fig. 13 that the lowest-lying bands in ^{186}Au should result from the coupling of quasiproton orbitals e and f ($\pi h_{9/2}$) with quasineutron orbitals A and B ($\nu i_{13/2}$).

3. *Signature splitting*

The energy splitting between the two signatures of a strongly coupled band can be a sensitive indicator of the quasiparticles involved. The application of this to bands in odd-odd nuclei has been discussed earlier [12,48]. As seen in the experimental Routhians of the odd-A neighbors (Fig. 13), the lowest-lying neutron bands (A, B) have a small signature splitting ($\Delta e' = 31$ keV for ^{185}Pt at $\hbar\omega = 0.2$ MeV), since the band is strongly coupled

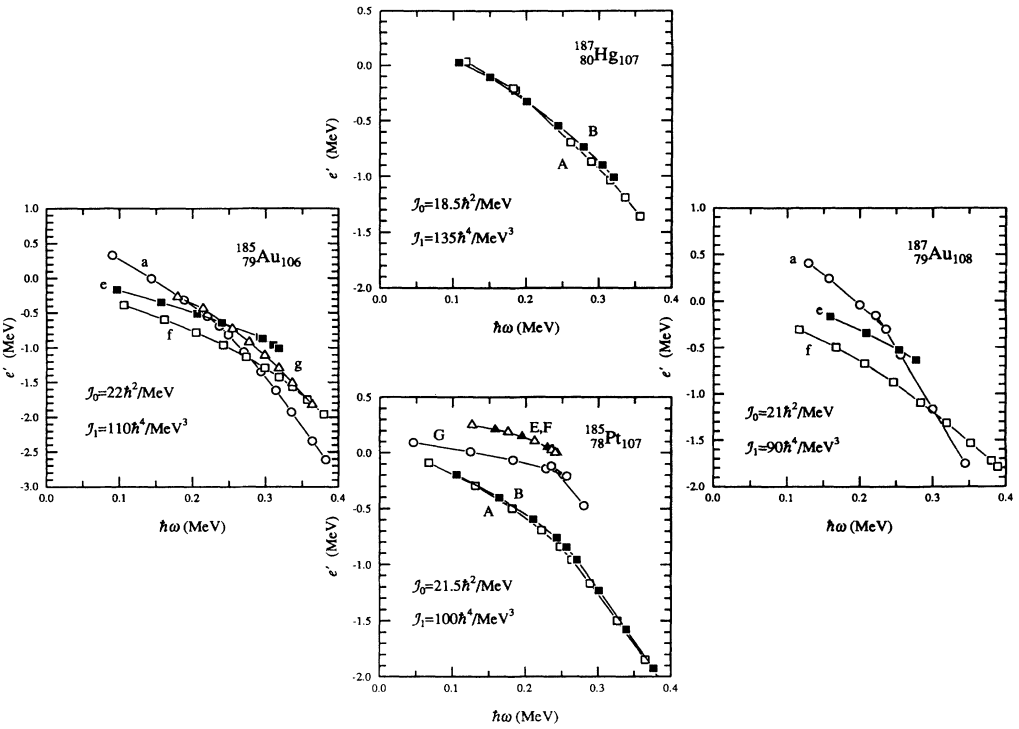

FIG. 13. Experimental quasiparticle Routhians for prolate configurations in the nuclei neighboring ^{186}Au. The data are taken from Refs. [10] (^{187}Hg), [6] (^{187}Au), [9] (^{185}Pt), and [1] (^{185}Au). In each case a reference due to the rotating core has been subtracted using the parameters shown. See Table IV for an explanation of the quasiparticle letter definitions.

($K = \frac{9}{2}$ initially). By comparison, the lowest proton bands (e, f) have a much larger value (265 keV for ^{185}Au and 324 keV for ^{187}Au at $\hbar\omega = 0.2$ MeV), since $K = \frac{1}{2}$.

Band 2 of ^{186}Au is seen to have some amount of signature splitting by the fact that the $\Delta I = 1$ transitions are not smoothly increasing in energy (see level scheme of Fig. 9). The degree of signature splitting can be measured quantitatively from the experimental Routhians for ^{186}Au shown in Fig. 14: $\Delta e' = 21$ keV at $\hbar\omega = 0.2$ MeV for band 2, and ≤ 5 keV for band 1. It is clear that the signature splitting of band 2 reflects the A, B value and thus that band 2 should be assigned as fA and fB, $\pi h_{9/2} \otimes \nu i_{13/2}$.

The consistency of the value of $\Delta e'$ for the A, B bands is illustrated in Fig. 15. The recently-measured value for ^{184}Ir [11] is included and is seen to be totally consistent with those measured for the $N = 107$ isotones. This lends confidence to the assignment of band 2 in ^{186}Au as configurations fA and fB. The A, B signature splitting is consistently larger at $N = 105$, and has a trend broadly similar to that for $N = 107$.

The observed signature splitting of band 1 in ^{186}Au is very small (Fig. 14), much less than $\Delta e'(A, B)$. It cannot be concluded from just this analysis as to whether this reflects the null E, F or a', b' splitting (the former is seen in Fig. 13, the latter is known to be small from measurements on ^{183}Ir, [4]). An alternative is that band 1 in ^{186}Au actually does have A, B as its neutron com-

TABLE IV. Definition of prolate quasiparticle configurations and Routhian labels used in the text. Capital letters and lower-case letters are used to distinguish neutron and proton excitations, respectively.

Routhian label	$(\pi, \alpha)^a$	Nilsson config. at $\hbar\omega = 0$	Dominant shell-model state
A	$(+, +\frac{1}{2})$	$\frac{9}{2}[624]$	$\nu i_{13/2}$
B	$(+, -\frac{1}{2})$		
E	$(-, +\frac{1}{2})$	$\frac{7}{2}[503]$	$\nu f_{5/2}$
F	$(-, -\frac{1}{2})$		
G	$(-, +\frac{1}{2})$	$\frac{1}{2}[521]$	$\nu p_{3/2}$
a	$(+, +\frac{1}{2})$	$\frac{1}{2}[660]$	$\pi i_{13/2}$
e	$(-, -\frac{1}{2})$	$\frac{1}{2}[541]$	$\pi h_{5/2}$
f	$(-, +\frac{1}{2})$		
g	$(-, -\frac{1}{2})$	$\frac{1}{2}[530]$	$\pi f_{7/2}$
a′	$(+, +\frac{1}{2})$	$\frac{5}{2}[402]$	$\pi d_{5/2}$
b′	$(+, -\frac{1}{2})$		

[a] The Routhian configurations are defined by their parity (π) and signature (α) quantum numbers. Band members have spins equal to α plus an even integer. For odd-A nuclei, $\alpha = \pm\frac{1}{2}$; for even-A, $\alpha = 0, 1$.

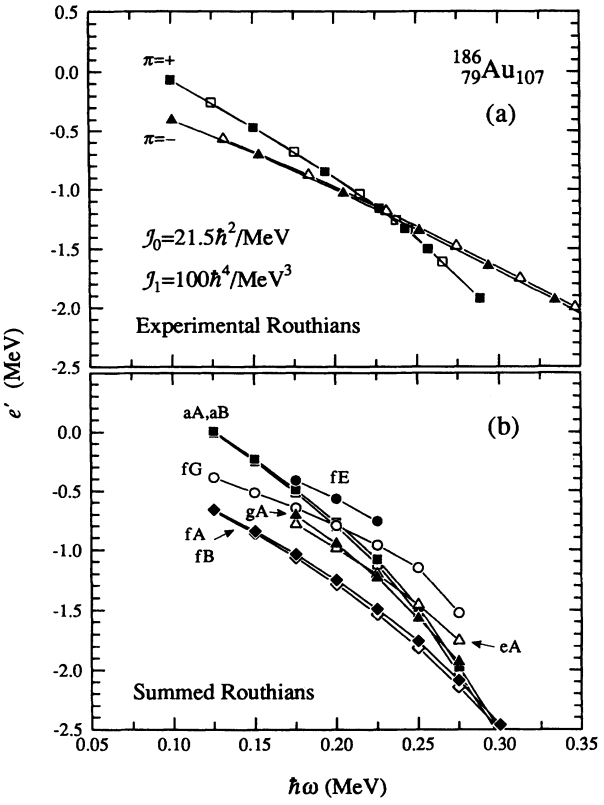

FIG. 14. (a) Experimental quasiparticle Routhians for prolate bands 1 (positive parity) and 2 (negative parity) in ^{186}Au. The core reference parameters are shown. (b) Odd-odd quasiparticle Routhians constructed by adding experimental one-quasiparticle Routhians of neighboring odd-A nuclei (see Fig. 13).

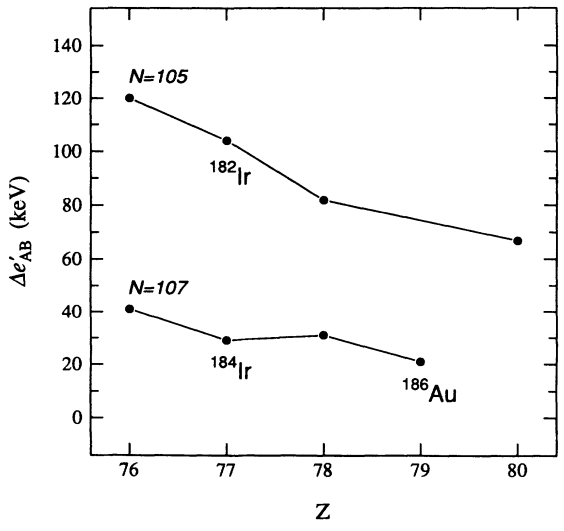

FIG. 15. Experimental energy splitting associated with the prolate $\nu i_{13/2}$ A, B signatures for $N = 105, 107$. The data are taken from Ref. [49] ($Z = 80$), the present work ($Z = 79$), Refs. [8,9] ($Z = 78$), Refs. [5,11] ($Z = 77$), and Refs. [50,51] ($Z = 76$).

ponent, but that the value of $\Delta e'$ is reduced by some nuclear structure effect such as the γ-driving tendency of the proton orbital, discussed in the following section.

4. *Summed Routhians*

The experimental one-quasiparticle Routhians (from the adjacent odd-A nuclei) can be summed directly to give an estimate of the expected Routhians for bands in an odd-odd nucleus. This procedure is carried out here for ^{186}Au utilizing the odd-A Routhians shown in Fig. 13. The experimental Routhians for proton configurations a, e, and f are averaged between ^{185}Au and ^{187}Au to yield representative values for $N = 107$, while the neutron A and B Routhians for ^{185}Pt and ^{187}Hg are averaged to give $Z = 79$ values. Since the prolate neutron configurations E, F, and G are not observed in ^{187}Hg [10], the averaged values for these three are taken to be higher than the averaged values for A and B by the same amount as they are in ^{185}Pt. These averaged proton and neutron Routhians are then summed to yield the odd-odd Routhians shown in Fig. 14.

The measured and summed Routhians in Fig. 14 can be compared directly. As expected, the lowest-energy configuration in both cases is the $\pi h_{9/2} \otimes \nu i_{13/2}$, fA and fB. At $\hbar\omega = 0.2$ MeV, the next highest summed Routhians are eA and eB, gA and gB, fG, aA, and aB, and fE and fF. (For clarity eB, gB, and gF are not included in Fig. 14.) As discussed in Sec. III B 4, positive parity is the preferred assignment for band 1 in ^{186}Au. In this case, the lowest available summed configuration is aA and aB, since fG has only one signature at that energy. The observed signature splitting of band 1 is very small ($\lesssim 5$ keV), whereas the summed aA and aB Routhians have exactly the A, B splitting (19 keV at $\hbar\omega = 0.2$ MeV). However, the $\pi i_{13/2}$ quasiparticle (orbital a) is expected to drive the nucleus strongly to positive values of the nuclear asymmetry parameter γ, which will have the result of reducing the signature splitting in a high-K band ($A, B; \frac{9}{2}[624]$). It is thus logical that band 1 have the aA, aB assignment ($\pi i_{13/2} \otimes \nu i_{13/2}$). By comparison, there is less γ driving due to the coupling with $\pi h_{9/2}$, since the proton Fermi surface lies within the $h_{9/2}$ shell.

If band 1 actually has negative parity, the lowest energy possibilities are eA, eB or gA, gB. The latter should retain the A, B splitting of the odd-N neighbors, since the g orbital is not expected to have a profound effect on the shape of the nucleus. And, the former should have splitting similar to that of the other $\pi h_{9/2} \otimes \nu i_{13/2}$ band, i.e., band 2. The marked difference in the signature splitting between bands 1 and 2 in the level scheme makes these negative-parity scenarios for band 1 unlikely.

The conclusion is that the most likely configuration for band 1 is $\pi i_{13/2} \otimes \nu i_{13/2}$ (aA and aB), based upon the adjacent odd-A nuclei. The ^{186}Au isotone ^{184}Ir has a positive-parity band that has been assigned $\pi d_{5/2} \otimes \nu i_{13/2}$ by Kreiner *et al.* [11]. However, a 5/2[402] $\pi d_{5/2}$ band is observed neither in ^{185}Au [1] nor in ^{187}Au [6], which makes it unlikely to appear at low energy in ^{186}Au.

The quasiparticle residual interaction is defined to be

the energy of the experimental Routhian minus the energy of the summed Routhian [52]. At $\hbar\omega = 0.2$ MeV, these values are +181 keV for fA, +171 for fB, and −210 for aA. One finds generally negative values (≈ -300 keV) for neutron-neutron residual interactions in the light Yb nuclei [52], indicative of the measured Routhian lying lower in energy than expected from a sum of single-quasiparticle components. While it is difficult to ascribe a great deal of significance to the absolute size of these residual-interaction values, the relative sizes of the interaction between different bands should be meaningful. Thus in ^{186}Au the 391-keV difference in this interaction for the fA and aA configurations is pertinent. That is, fA (band 2) lies higher in energy than expected from the sum, aA (band 1) lower. It is not clear why this should happen. Garrett *et al.* [53] have discussed cases where the residual interaction is anomalously positive due to the poor overlap of the orbital wave functions of high-K versus low-K states. However, the proposed configurations of bands 1 and 2 both involve a high-K orbital ($\nu i_{13/2}$: $\frac{9}{2}$[624]) coupled to a low-K ($\pi h_{9/2}$: $\frac{1}{2}$[541] and $\pi i_{13/2}$: $\frac{1}{2}$[660]). It is not understood then why the residual interactions for bands 1 and 2 differ by 0.4 MeV.

5. *Quasiparticle alignments*

The quasiparticle angular momentum aligned with the axis of rotation, i, is calculated from the total angular momentum of the level after a reference angular momentum is subtracted to account for the rotational component. These alignments are plotted as a function of rotational frequency in Fig. 16 for ^{186}Au and its neighbors. One notes crossings in most of the bands due to the alignment of additional quasiparticles, but first one should consider the alignments before any crossings have occurred.

Just as we discussed additivity of quasiparticle energies in the previous section, the aligned angular momenta of single-quasiparticle states approximately add to reproduce alignments in odd-odd bands. From Fig. 16, it is clear that i is approximately $4\hbar$ to $5\hbar$ for the $\pi h_{9/2}$ band f in ^{185,187}Au and for the $\nu i_{13/2}$ bands A and B in ^{185}Pt and ^{187}Hg (at $\hbar\omega = 0.2$ MeV). Thus, the alignment of configuration fA (band 2) in ^{186}Au should be $8\hbar$ to $10\hbar$, if there were no residual interactions. The fact that i of band 2 in ^{186}Au is only $6.5\hbar$ at this frequency is another indication of the sizeable residual interaction in this configuration (as also indicated by the discussion on summed Routhians in the previous section). The comparable band in the isotone ^{184}Ir has an identical alignment of $6.5\hbar$ [11].

By comparison, band 1 in ^{186}Au has a larger initial aligned angular momentum, $i \simeq 9\hbar$ at $\hbar\omega = 0.2$ MeV. This is logical, since the $\pi i_{13/2}$ band a in ^{185}Au and ^{187}Au has $i \simeq 7\hbar$, $2.5\hbar$ to $3\hbar$ larger than that of configuration f. It is thus reasonable that $i(aA)$ be $2.5\hbar$ to $3\hbar$ larger than

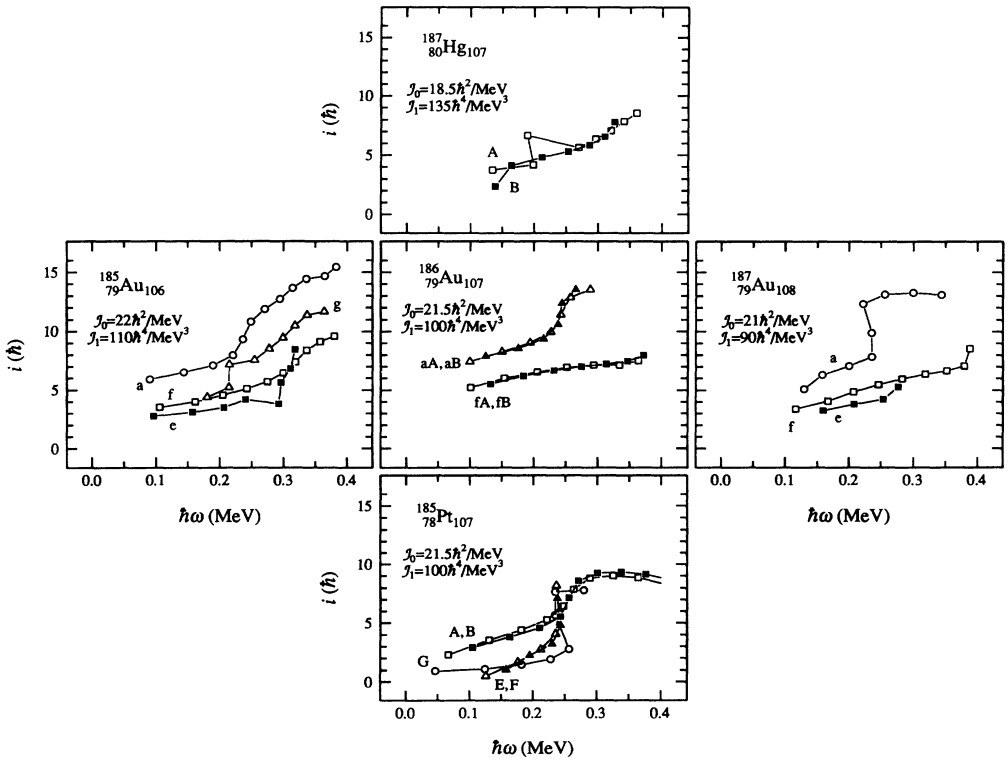

FIG. 16. Aligned quasiparticle angular momentum i as a function of rotational frequency for prolate bands in ^{186}Au and neighboring nuclei. In each case an aligned spin due to the rotating core has been subtracted using the parameters shown. The data references are listed in the caption of Fig. 13.

$i(fA)$ in ^{186}Au, as is observed. No other combination of two quasiparticles near to the Fermi surface could yield such a high degree of alignment.

6. *Band crossings*

As is seen in Fig. 16, band 2 in ^{186}Au has no band crossing, whereas band 1 has a clear alignment process at $\hbar\omega = 0.23$ MeV. A simple blocking argument suggests that the alignment of $h_{9/2}$ protons is responsible, since a crossing is present in the $\pi i_{13/2} \otimes \nu i_{13/2}$ (aA, aB) configuration, but is absent in $\pi h_{9/2} \otimes \nu i_{13/2}$ (fA, fB). The expected low-frequency $\nu i_{13/2}$ crossing is blocked in both.

A more systematic analysis yields the same conclusion of a low-frequency $\pi h_{9/2}$ crossing in the Au isotopes, as discussed by Carpenter *et al.* [7]. Generally the alignment of $h_{9/2}$ protons occurs at $\hbar\omega \geq 0.4$ MeV in this region, according to cranked shell-model calculations [7]. However, in the special case characterized by positive γ deformation and reduced proton pairing, this $\pi h_{9/2}$ crossing can come low in frequency. Both of these conditions are satisfied in band a of ^{185,187}Au and aA of ^{186}Au. The $\pi i_{13/2}$ orbital a strongly drives the nucleus to positive γ (cf. Ref. [7]), and in addition blocks a significant amount of the proton pairing. Thus, it is reasonable that the $\pi h_{9/2}$ crossing can occur at $\hbar\omega < 0.3$ MeV in these three bands in Au nuclei.

By comparison, it is more difficult to arrive at a clear interpretation of the crossings at $\hbar\omega = 0.25$ MeV in ^{185}Pt. A measurement of $M1/E2$ ratios in bands A and B of ^{185}Pt [4] shows the matrix element ratios rising dramatically as a result of the band crossing, which is indicative of a proton rather than a neutron crossing affecting the $M1$ transition rates. These data strongly indicate that a low-frequency $\pi h_{9/2}$ crossing is present also in ^{185}Pt.

However, it is possible to advance arguments in favor of a different crossing scenario at $N = 107$, as discussed in Ref. [7]. The alternative approach depends heavily on the proposed shape-driving characteristics of orbitals near the Fermi surface, within the cranked shell model. The configurations of the single-quasiparticle states in ^{185}Pt are A and B $(\nu i_{13/2})$, E and F $(\nu f_{7/2})$, and G $(\nu p_{3/2})$. All are expected to drive the nucleus at least slightly to negative γ, which would keep the $\pi h_{9/2}$ crossing at high frequency. The crossings in ^{185}Pt would then be AB $(\nu i_{13/2})$ in bands E, F, and G, and BC, AD in bands A, B, by this line of reasoning [7]. Differences in γ between these bands would allow the crossing frequencies for AB and BC, AD to be similar, although the $B(M1)/B(E2)$ results would then be extremely difficult to interpret.

Nevertheless, regardless of the two possibilities for ^{185}Pt, it is logical to assign the crossing in band 1 of ^{186}Au to the $\pi h_{9/2}$ alignment process. This and the corresponding crossing in the $\pi i_{13/2}$ band of ^{187}Au [6] are two cases where the controversial $\pi h_{9/2}$ crossing can be clearly identified. Discussion of this crossing in neighboring nuclei is also given in Ref. [12].

B. Oblate bands

In order to facilitate the discussion of quasiparticle properties in the oblate systems, we have labeled individual Routhians closest to the Fermi surface by letter designations, just as in the prolate discussion. The correspondence between those labels, the parity and signature, asymptotic Nilsson quantum numbers and shell-model origins is outlined in Table V. Within the cranked shell model only the parity and signature are valid labels under rotation, strictly speaking. However, the high-j $\pi h_{11/2}$ and $\nu i_{13/2}$ designations are fairly good approximations. In the following subsections, two-quasiparticle states are labeled according to $\nu \otimes \pi$ configurations, in order to differentiate between oblate and prolate bands (the latter were labeled $\pi \otimes \nu$ in the previous subsections).

As already discussed, the most visible band structures in the odd-odd $^{186-194}$Au isotopes are those built on isomeric 11^- states, having a $\nu i_{13/2}^{-1} \otimes \pi h_{11/2}^{-1}$ configuration. Due to the large energy difference between the signatures of the $K = \frac{1}{2}$ $h_{11/2}$ orbital, the two lowest sequences will have an $\alpha = -\frac{1}{2}$ $h_{11/2}$ proton coupled to each of the neutron $i_{13/2}$ signatures, i.e., the Ae and Be combinations.

These bands have a number of distinguishing features, including a pronounced energy staggering between levels of odd and even spin, and a clear reversal of the sign of that staggering at higher spins. There are also indications of the onset of a band crossing at the highest spins observed. In addition, the 11^- band in ^{188}Au is crossed by a highly aligned structure, with a small interaction. A discussion of the $B(M1)/B(E2)$ matrix element ratios will be deferred until Sec. IV C.

TABLE V. Definition of oblate quasiparticle configurations and Routhian labels used in the text. Capital letters and lower-case letters are used to distinguish neutron and proton excitations, respectively.

Routhian label	(π, α)[a]	Nilsson config. at $\hbar\omega = 0$	Dominant shell-model state
A	$(+, +\frac{1}{2})$	$\frac{7}{2}[633]$	$\nu i_{13/2}$
B	$(+, -\frac{1}{2})$		
C	$(+, +\frac{1}{2})$	$\frac{5}{2}[642]$	$\nu i_{13/2}$
D	$(+, -\frac{1}{2})$		
E	$(-, +\frac{1}{2})$	$\frac{3}{2}[512]$	$\nu p_{3/2}$
F	$(-, -\frac{1}{2})$		
G	$(-, +\frac{1}{2})$	$\frac{5}{2}[503]$	$\nu f_{5/2}$
H	$(-, -\frac{1}{2})$		
e	$(-, -\frac{1}{2})$	$\frac{1}{2}[501]$	$\pi h_{11/2}$
f	$(-, +\frac{1}{2})$		
a	$(+, -\frac{1}{2})$	$\frac{1}{2}[431]$	$\pi d_{3/2}$
b	$(+, +\frac{1}{2})$		

[a] See footnote to Table IV.

1. Signature inversion

Figure 17 illustrates the energy differences between consecutive spin levels, showing the clear odd-even staggering for the 11^- bands in the $N = 107 - 113$ Au isotopes. A change in phase at intermediate spins can be seen in all cases. That is, the $I = 16, 18$, and 20 members are shifted to lower energy (relative to the odd-I states), but at lower spins it is the odd-I states (11 and 13) that lie lower. Within the cranked shell model (CSM) such a phase reversal is expressed as a change of sign in the energy splitting between rotational signatures. This signature inversion effect has been cited by Bengtsson *et al.* [54] and Dönau and May [55] as a strong indication of stable triaxiality under the usual rotation about the shortest symmetry axis. More recently, though, Ikeda and Shimano [56] have interpreted the phenomenon as due to γ *fluctuations* around an axially symmetric equilibrium deformation, using a reversed γ dependence of the moments of inertia.

Some of the most well-known examples of this behavior are the odd-odd rare-earth nuclei having $N \simeq 90$. There the inversion has been linked [54] to the competition between the γ driving influences of $K = \frac{1}{2}$ $i_{13/2}$ neutrons and $K = \frac{5}{2}$ $h_{11/2}$ protons, resulting in well-defined triaxial deformations. By comparing the experimental inversion frequencies and signature splitting to Nilsson CSM calculations, Bengtsson *et al.* [54] were able to extract ε_2 and γ deformations in a number of odd-odd rare-earth nuclei. The resulting γ deformations fell into the range 5° to 25°.

In the odd-odd Au isotopes the same high-j orbitals are involved but the details of the story are quite different. For these oblate nuclei undergoing collective rotation ($\gamma \simeq -60°$) the Fermi surface lies at the top of the proton $h_{11/2}$ subshell, while it is near the middle of the neutron $i_{13/2}$ shell. These placements correspond to K values of approximately $\frac{1}{2}$ for the protons and $\frac{7}{2}$ for the neutrons.

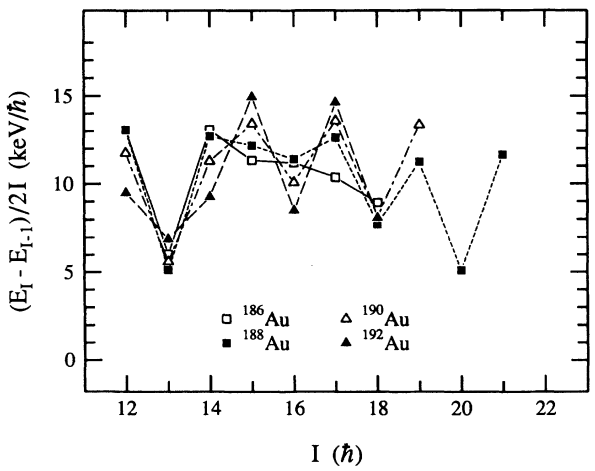

FIG. 17. Energy staggering between odd and even spins for oblate 11^- bands in ^{186,188}Au (present work) and ^{190,192}Au [17].

Under these conditions the valence high-j proton tends to push the nuclear deformation toward $\gamma = -120°$, while the neutron prefers an intermediate γ deformation of $\gamma \simeq -50°$ [55,57]. If the proton influence is strong enough to drive the equilibrium deformation away from oblate symmetry ($\gamma = -60°$) in the direction of $-120°$, the normally unfavored $\nu i_{13/2}$ $\alpha = -\frac{1}{2}$ signature lies lower in energy than the $\alpha = +\frac{1}{2}$ signature over some finite range of rotational frequency. As a result, at low frequency the energetically favored signature of the odd-odd $\nu i_{13/2}^{-1} \otimes \pi h_{11/2}^{-1}$ configurations could have the anomalous value of $\alpha_T = \alpha_\nu + \alpha_\pi = \mathrm{mod}[-\frac{1}{2} + (-\frac{1}{2})] = 1$.

Figure 18 shows the experimentally observed frequencies below which the normally unfavored signature is lowest in energy for these bands in $^{186-194}$Au. The signature inversion frequencies are strongly dependent on neutron number, unlike the $\nu i_{13/2}$ band-crossing frequencies for the core Hg isotopes which are also shown. The theoretical Routhians for neutron and proton quasiparticles in an oblate potential are shown in Fig. 19, including an expanded view of the quasineutron Routhians using identical parameters except for $\gamma = -70°$ instead of $-60°$. As Bengtsson *et al.* [54] have indicated, pure rotation about a major but nonsymmetry axis (here $\gamma = -60°$) cannot produce a signature inversion. However, for $\gamma = -70°$ the normally unfavored $\alpha = -\frac{1}{2}$ component is lowest in energy at frequencies below the first band crossing.

The theoretical inversion frequency can be extracted from the Routhians in Fig. 19(a) if the weak-interaction band crossing at $\hbar\omega = 0.20$ MeV is removed. The resulting value of 0.22 MeV is clearly less than the experimental frequency of 0.35 MeV for ^{186,188}Au, and more in line with the values extracted for the heavier isotopes (see

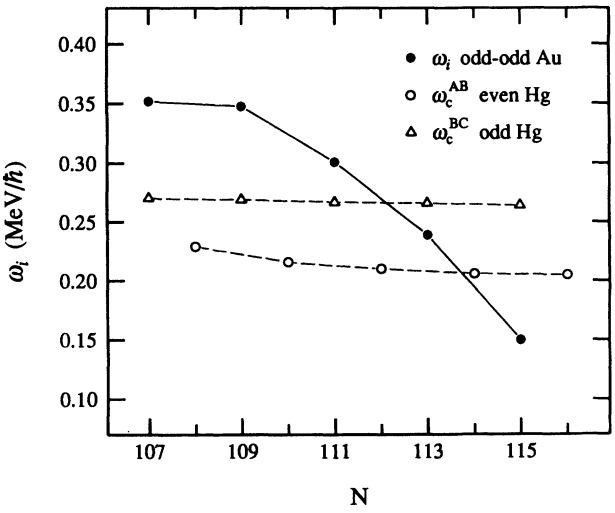

FIG. 18. Signature inversion frequencies for oblate 11^- bands in $^{186-194}$Au (present work and Ref. [17]; the value for ^{194}Au is the result of an extrapolation from higher frequencies). Also shown for comparison are the measured band-crossing frequencies for the $\nu i_{13/2}$ alignments (AB and BC) in these oblate bands, taken from Refs. [10,58] (even-A Hg) and Refs. [10,58,59] (odd-A Hg isotopes).

Fig. 18). In principle a similar analysis to that accomplished in Ref. [54] could be performed over a range of (β_2, γ) deformations, in order to match the experimental inversion frequencies and signature splittings with theory. However, such a procedure is more difficult in this region, since the calculated effect is more sensitive to the deformation parameters here than in the rare-earth nuclei, and it is necessary to reliably remove the band crossings occurring in the theory at low frequencies. It is not clear that the standard cranked shell-model approach, based on a stable triaxial deformation, is capable of quantitatively explaining the experimental signature-inversion characteristics. It would be interesting to see if the alternative picture of γ vibrations coupled to a "γ-reversed" rotation [56] can account for the observed inversion effect in these oblate gold nuclei.

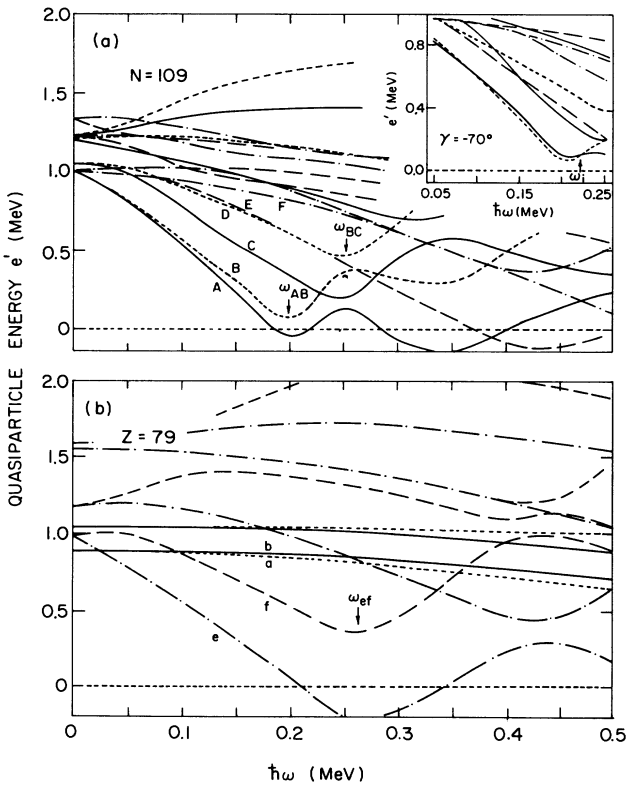

FIG. 19. Theoretical Routhians for (a) neutrons and (b) protons, calculated using the Woods-Saxon cranked shell model assuming oblate shapes. The parameters are as follows: $\beta_2 = 0.16$, $\beta_4 = -0.03$, $\gamma = -60°$, $\Delta^\nu(\omega = 0) = 0.992$ MeV, and $\Delta^\pi(\omega = 0) = 0.683$ MeV. The constant pairing value is taken to be 85% of the BCS-calculated pairing at $\hbar\omega = 0$. The letter designations are based on parity, rotational signature, and energy order, and are listed in Table IV. Band-crossing frequencies have been marked, corresponding to the rotational alignment of the lowest $i_{13/2}$ (ω_{AB}) quasineutron, second-lowest $i_{13/2}$ (ω_{BC}) quasineutron, and lowest $h_{11/2}$ (ω_{ef}) quasiproton pairs. The inset in panel (a) shows the theoretical neutron Routhians for $\gamma = -70°$, on an expanded scale. The inversion of the A, B $\nu i_{13/2}$ signatures can be seen at low frequency.

2. *Band crossings*

The quasiparticle alignments i are plotted in Fig. 20 as a function of rotational frequency for the known oblate bands in odd-odd $^{186-192}$Au. As in the prolate cases it should be possible to compare the neighboring odd-A oblate bands to the odd-odd Au structures. The $\pi h_{11/2}$ bands in the odd-A Au isotopes are well known and have an initial alignment of $i(\pi) \simeq 4.2\hbar$ [6]. The $\nu i_{13/2}$ bands in odd-A Hg nuclei have also been well established and reveal $i(\nu) \simeq 6.2\hbar$ [9]. The resultant sum $i(\nu) + i(\pi) \simeq 10.4\hbar$ agrees well with the observed initial alignment of $i(\nu \otimes \pi) \simeq 10.1\hbar$ for the $\nu i_{13/2}^{-1} \otimes \pi h_{11/2}^{-1}$ bands in ^{186,188}Au.

There are at least beginnings of band crossings observed in each of the odd-odd Au nuclei exhibited in Fig. 20. The most complete crossing occurs in ^{188}Au between bands 1 and 2 (see Fig. 8). The angular distribution measurements lead to the conclusion that the two structures are connected by stretched quadrupole transitions and thus that a rotation alignment process occurs. The dotted lines for the negative-parity states in ^{188}Au (Fig. 20) represent this band 1 and 2 relationship and indicate a sharp backbend at $\hbar\omega = 0.31$ MeV. However, the continuation of the levels in band 2 of ^{188}Au gives rise to perhaps another crossing (denoted by solid lines in Fig. 20) at $\hbar\omega \simeq 0.35$ MeV. There is the beginning of a crossing in the negative-parity bands of the other Au isotopes in Fig. 20. These may resemble more the "second" crossing in ^{188}Au, since the $\Delta I = 1$ transitions are present throughout (note that they are not observed in the band 1 to band 2 crossing in ^{188}Au). Of course, the primary $\nu i_{13/2}$ crossing (AB) is blocked in each of these bands.

Theoretical Routhians from the Woods-Saxon cranked shell model are shown in Fig. 19. Compared to prolate band crossings in this region, the oblate $\nu i_{13/2}$ alignments occur at markedly lower frequencies, a direct consequence of the smaller oblate moment of inertia and correspondingly larger Coriolis force responsible for decoupling the quasineutron pair. In addition, the interaction between bands is predicted to be small, of the order of 40 keV for the AB crossing. This gives rise to the extremely sharp crossings with large gains in alignment which are well known in neighboring nuclei [6,10,58]. The alignment of $h_{11/2}$ quasiprotons is predicted to occur higher in frequency than several neutron alignments; there is some evidence for its occurrence at the highest spins observed in the heavier Hg isotopes, $I \simeq 28$ [58].

The $\nu i_{13/2}$ AB crossing is blocked in the $\nu i_{13/2}^{-1} \otimes \pi h_{11/2}^{-1}$ configuration, and the second $\nu i_{13/2}$ crossing (BC, AD) is predicted to occur slightly higher in frequency, with a larger interaction and somewhat less of an alignment gain than the AB crossing (Fig. 19). We propose that the sharp crossing in ^{188}Au ($\hbar\omega = 0.31$ MeV, $\Delta i \simeq 7.6\hbar$) results from the secondary $\nu i_{13/2}$ alignment. By comparison, this BC crossing is observed in the oblate $\nu i_{13/2}$ bands of odd-A Hg isotopes at approximately 0.27 MeV, with a typical gain in alignment of $\Delta i \simeq 8.4\hbar$ [10,59]. The γ deformation of the odd-odd Au nuclei is expected to be slightly *more* negative than $\gamma = -60°$ (see the previous discussion on signature inversion effects). Due to the $\nu i_{13/2}$ γ-driving influence, the odd-A Hg bands likely

have a γ deformation *less* negative than $\gamma = -60°$. This difference would lead to a somewhat higher BC crossing frequency in the odd-odd Au nuclei than in the odd-A Hg isotopes.

Concerning the systematically occurring but only partially observed crossing in the negative-parity bands of odd-odd Au nuclei (Fig. 20), one possibility is that they represent the next possible $\nu i_{13/2}$ alignments, i.e., $Ae \rightarrow AeCD$ and $Be \rightarrow BeAD$. The CD crossing is reported at $\hbar\omega = 0.35$ MeV in even-even $^{188-194}$Hg [10,58], with a larger interaction strength than the initial AB alignment. It is possible that such a CD, AD crossing may be occurring in the $\nu i_{13/2}^{-1} \otimes \pi h_{11/2}^{-1}$ band of each odd-odd Au isotope shown in Fig. 20.

3. Oblate 15^+ bands

The presence of 15^+ and 17^+ states, decaying *via* high-energy $E1$ transitions to the oblate 11^- bands, is a systematic feature of the odd-odd Au isotopes [17]. For $N = 111 - 115$ these states have been characterized as $\nu i_{13/2}^{-1} \otimes \pi h_{11/2}^{-1}$ excitations coupled to known 5^- and 7^- states in the oblate Hg core nuclei. According to Neskakis *et al.* [17], the result is a $\nu i_{13/2}^{-2} \otimes \pi h_{11/2}^{-1} \otimes$"$\nu j$" four-quasiparticle configuration, where the last quasineutron is taken to originate from the shell-model $p_{1/2}$, $p_{3/2}$, or $f_{5/2}$ states. For ^{186,188}Au ($N = 107, 109$) the latter two configurations are the most likely, as listed in Table V, and therefore the 15^+ bands represent $ABeE, ABeF$, or $ABeG, ABeH$ combinations. In ^{188,190}Hg the AE, AF bands have an initial alignment $i_{AE} \simeq 8.2\hbar$. Adding this to the known odd-odd Be alignment ($i_{Be} \simeq 10.6\hbar$) results in a total alignment of $18.8\hbar$, to be compared with the experimental value of approximately $16.7\hbar$ observed in ^{188}Au (Fig. 20).

The "bottoms" of these bands show the odd spins of 15^+ and 17^+ being favored, which have $\alpha_T = 1$. However, at higher spins the bands seem to undergo somewhat of a rearrangement and the even spins ($\alpha_T = 0$) become favored, although the spin assignments are less conclusive in these excited structures. It is not possible to put forward a definitive explanation, but such a switch is consistent with the band starting out with a $p_{3/2}$ neutron as the fourth quasiparticle ($\alpha = -\frac{1}{2}$ lowest in energy), and then changing to an $f_{5/2}$ quasiparticle ($\alpha = +\frac{1}{2}$ lowest) at larger rotational frequency.

C. $B(M1)/B(E2)$ measurements

In this section, an analysis of the γ-ray branching ratios is given for both the prolate and oblate bands. The use of $B(M1)/B(E2)$ ratios for bands involving a single quasiparticle, or a single quasiparticle plus a pair of aligned quasiparticles, has proven to be quite useful in characterizing the specific orbitals involved (see, for example, Refs. [4,12,60,61]). The extension of the theoretical mod-

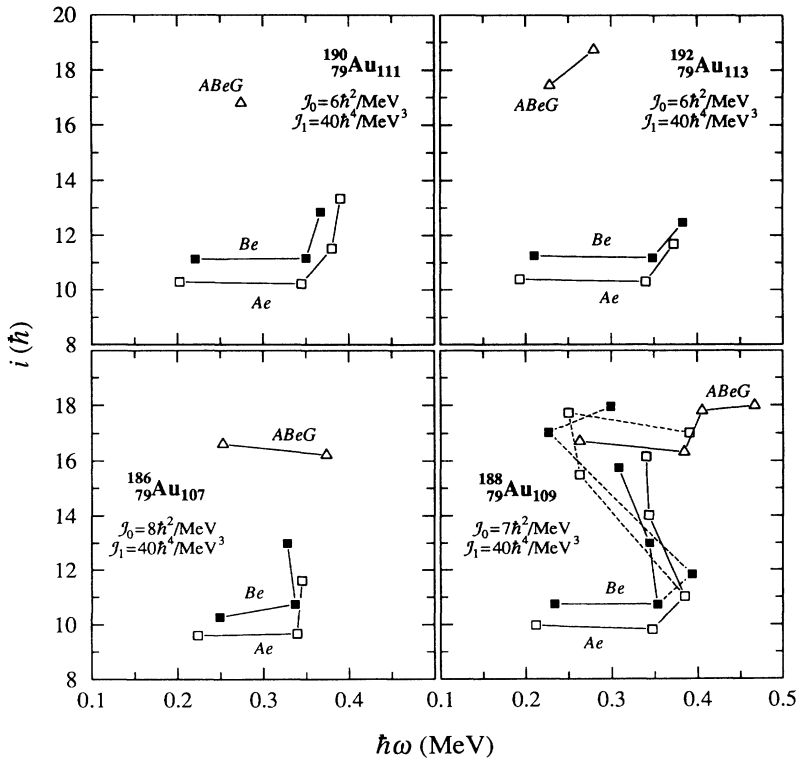

FIG. 20. Quasiparticle aligned angular momentum i vs rotational frequency for oblate bands in $^{186-192}$Au (present work and Ref. [17]). The rotational core parameters are indicated.

els to two- and four-quasiparticle bands has not received as much attention (however, see Refs. [62–65]). Our approach here is derived from the semiclassical treatment by Dönau and Frauendorf [14,15].

Many two-quasiparticle configurations for which clear $\Delta I = 1$ transitions are observed involve one orbital which has a modest energy splitting between the two signatures, combined with a second orbital which has a substantially larger signature splitting. The energetically favorable configuration in such a case involves *both* signatures of the former orbital coupled to *one* signature of the latter (the one lower in energy). Therefore we use an approach where the quasiparticle which contributes both its signatures is the "signature-active" participant, and the other quasiparticle is the "signature-spectator" partner.

The consequences of this are twofold. First, the signature splitting of the two-quasiparticle band in an even-A nucleus is expected to reflect the signature splitting of the "signature-active" one-quasiparticle band in the adjacent odd-A nuclei, as already discussed. Second, because we are working within a principal-axis cranking formalism and signature is considered to be a good quantum number, the $M1$ transition matrix element contains more terms associated with the "signature-active" participant than with the "signature-spectator" partner.

The standard geometric formalism for the $B(M1)$ values [14,15] can be extended for the case of two quasiparticles:

$$B(M1;\, I \to I-1) = \frac{3}{8\pi}\frac{1}{I^2}[\,(g^{(1)} - g_R)(k^{(1)}\sqrt{I^2-K^2} - i^{(1)}K \pm \Delta e'/\omega) - (g^{(2)} - g_R)i^{(2)}K - (g^{(3)} - g_R)i^{(3)}K]^2\,\mu_N^2, \tag{2}$$

where superscript (1) denotes the "signature-active" participant, which has both signatures involved, and superscript (2) refers to the "signature spectator" partner, which has only one signature taking part in the two-quasiparticle coupling. The most significant change to the original geometric model [14,15] is that we allow an additional term proportional to the alignment of quasiparticle (2). The superscript (3) refers to an additional pair of quasiparticles that undergo an alignment due to rotation.

The above expression also contains a term arising from the signature splitting ($\Delta e'$) that leads to a staggering of the $B(M1)$ values, just as it does in the one-quasiparticle case. The phase is defined [15] such that the $M1$ matrix element is enhanced for the transition energy $E_\gamma \simeq \hbar\omega - \Delta e'$, and diminished for $E_\gamma \simeq \hbar\omega + \Delta e'$, where $\Delta e'$ is the energy difference between the two signatures in the rotating frame and is extracted from experiment. This definition is *directly* related to the phase of the signature splitting, and as a result, for the two-quasiparticle configurations under consideration the staggering of the $B(M1)/B(E2)$ ratios is expected to follow the energy staggering. The present work provides a clear test of that prediction, since the energy splitting in the prolate bands is opposite in phase to that of the oblate bands. Note that although Eq. (2) is exact only for axially symmetric nuclei, it is certainly a good approximation for γ near 0° (which is likely the case for all bands seen here).

The $B(E2)$ matrix element is expressed in the well-known "geometrical" manner:

$$B(E2;\, I \to I-2) = \frac{5}{32\pi}Q_0^2\cos^2(\gamma + 30°)\left[1 - \left(\frac{K}{I-1}\right)\right]^2 (e\,\mathrm{b})^2\,. \tag{3}$$

For the Au bands built on prolate shapes, we rely on the measured $B(E2)$ value [66] in the even-even ^{184}Pt to give the "core" degree of $E2$ collectivity in this region. This core $B(E2)$ value is modified slightly for various quasiparticle states according to the results of calculations of the total Routhian surfaces (TRS) [7]. That is, we assume that Q_0 is directly proportional to β_2 and scale the core value of Q_0 by the calculated β_2 values. The TRS results are $\beta_2 = 0.23$ for the prolate core, 0.22 for the prolate $\pi h_{9/2} \otimes \nu i_{13/2}$ configuration (^{186}Au), 0.25 for the prolate $\pi i_{13/2} \otimes \nu i_{13/2}$ configuration (^{186}Au), and 0.17 for the ^{186,188}Au oblate bands. We also assume axial symmetry for each of these cases.

The experimental $B(M1)/B(E2)$ values are determined using the standard approach:

$$\frac{B(M1;\, I \to I-1)}{B(E2;\, I \to I-2)} = 0.693\,\frac{E_\gamma^5\,(I \to I-2)}{E_\gamma^3\,(I \to I-1)}\,\frac{1}{\lambda(1+\delta^2)}\left(\frac{\mu_N}{e\,\mathrm{b}}\right)^2. \tag{4}$$

The branching ratios, λ, are taken from the γ-ray intensities of Tables I and II. As discussed in Sec. II, estimates of the $E2/M1$ mixing ratios δ have been obtained only for the most intense transitions. Average mixing ratios of 0.2 ($\pi h_{9/2} \otimes \nu i_{13/2}$ prolate), 0.2 ($\pi i_{13/2} \otimes \nu i_{13/2}$ prolate) and 0.0 ($\nu i_{13/2}^{-1} \otimes \pi h_{11/2}^{-1}$ oblate) have been used. Since these values enter into Eq. (4) as $1/(1+\delta^2)$, their effect is not large.

1. Prolate negative-parity band in ^{186}Au

The experimental values of $B(M1)/B(E2)$ for the prolate negative-parity band ($\pi h_{9/2} \otimes \nu i_{13/2}$) in ^{186}Au are shown in Fig. 21(a). Above $I = 12$ the ratios average approximately 0.55 $(\mu_N/e\,\mathrm{b})^2$, with a consistent odd-even staggering. Also shown in Fig. 21(a) are the theoretical values obtained using the geometrical approach. It is not understood why the experimental points below $I = 12$

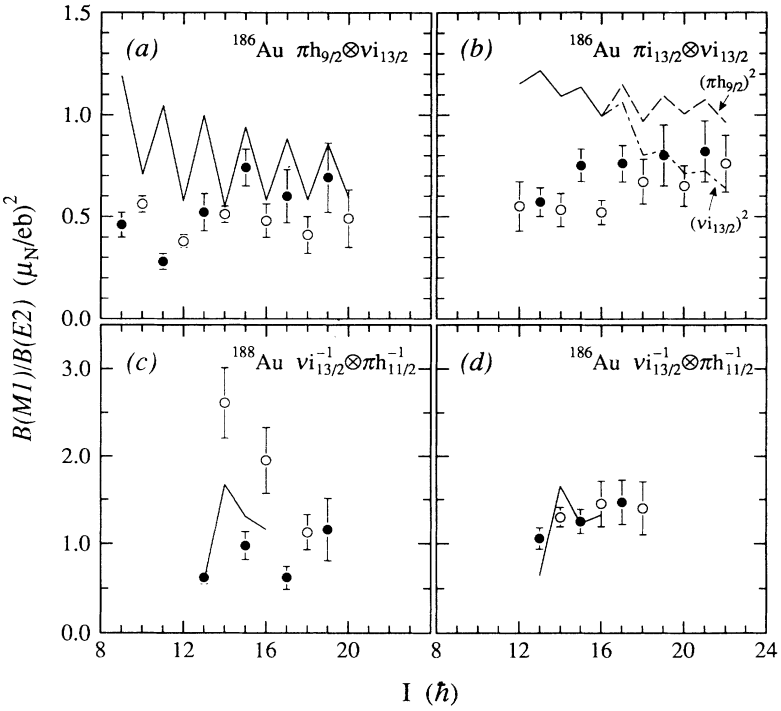

FIG. 21. Ratios of reduced transition probabilities for prolate [(a) and (b)] and oblate [(c) and (d)] bands in ^{186,188}Au. The solid lines represent the theoretical estimates, using the following parameters (see text also): $g_K - g_R$ $(\pi h_{9/2}) = 0.336$; $g_K - g_R$ $(\pi i_{13/2}) = 0.824$; $g_K - g_R$ $(\nu i_{13/2}) = -0.605$; $g_K - g_R$ $(\pi h_{11/2}) = 0.865$; $Q_0 = 5.8$ e b (prolate) [66] and $Q_0 = 4.5$ e b (oblate). Inclusion of a band crossing in part (b) gives either the dashed ($\pi h_{9/2}$ alignment) or dot-dashed line ($\nu i_{13/2}$ alignment).

have a phase opposite to the theory. There is no appreciable alignment gain observed for this band, since both primary band crossings in this region are blocked. Although the average calculated $B(M1)/B(E2)$ is somewhat high, there is good agreement with the experimental ratios above $I = 12$. In particular, the phase and magnitude of the staggering are reproduced.

2. *Prolate positive-parity band in ^{186}Au*

Experimental and theoretical $B(M1)/B(E2)$ values are shown in Fig. 21(b) for the prolate positive-parity band in ^{186}Au. A small but consistent odd-even staggering, with the same phase as in the other prolate band, can be seen in the experimental data above $I = 13$. Again the magnitude and phase of the staggering are reproduced by the calculation, although on average the theoretical ratios are somewhat higher than the experimental values.

A sharp crossing, due to the alignment of $h_{9/2}$ protons, is observed in this band (see Fig. 16). There is essentially no effect on the $B(M1)/B(E2)$ ratios [Fig. 21(b)]. This is consistent with a $\pi h_{9/2}$ alignment, because the moderate increase in the $M1$ matrix element due to a proton crossing is opposed by (a) a slight decrease in $B(M1)$ as a function of spin due to contributions from the other quasiparticles, and (b) a slight increase in $B(E2)$ due to the β_2-driving influence of the $h_{9/2}$ protons. Alternatively, a decrease in the $M1$ rate caused by a neutron crossing is reinforced by (a) and (b). Therefore, as shown in Fig. 21(b), the rather constant nature of the experimental $B(M1)/B(E2)$ ratios is consistent with the inclusion of a proton as opposed to a neutron crossing in the calculation.

3. *Oblate 11^- bands in ^{186,188}Au*

As discussed earlier, the staggering of the energy levels is a well-known feature in $^{186-194}$Au, and the unusual signature splitting pattern has been interpreted in terms of a slightly triaxial deformation [54,55]. The measured oblate $B(M1)/B(E2)$ values are shown in Figs. 21(c) and 21(d) for the oblate bands in ^{186,188}Au. The odd-even staggering is quite large in ^{188}Au, as it is in the heavier isotopes [17]. The averaged theoretical values are in good agreement with the data, but it is not possible to reproduce the magnitude of the experimental odd-even staggering. Reliable $B(M1)/B(E2)$ values could not be measured above the sharp crossing in the oblate band in ^{188}Au.

Note that the low-spin phase of the $B(M1)/B(E2)$ staggering is identical to that of the energy staggering, and is opposite to that in the prolate structures. This is consistent with the description of the band as consisting of two signature partners with the same configuration. There does seem to be a decrease in the amount of $B(M1)/B(E2)$ oscillation, although it occurs more gradually than the quickly "damped" behavior seen in the theory.

The smoothness of the $B(M1)/B(E2)$ ratios for the oblate band in ^{186}Au marks a sudden departure from the pronounced staggering in the heavier isotopes. Since the signature splittings in ^{186}Au and ^{188}Au are comparable, the theoretical $B(M1)/B(E2)$ staggering is also similar in the two cases, clearly not in agreement with the data. However, the averaged theoretical values agree reasonably well with experiment, and for ^{188}Au the overall agreement is somewhat improved over the calculations of Toki *et al.* [67] for the heavier odd-odd Au isotopes.

In summary, on the one hand the calculations described here reproduce the *average* $B(M1)/B(E2)$ ratios for the oblate configurations, but not the magnitude of the observed staggering. On the other hand, for the prolate configurations the odd-even staggering is well represented by the theory, while the overall $B(M1)/B(E2)$ magnitude is slightly too high.

V. SUMMARY

The present work has investigated rotational band structures in odd-odd ^{188}Au and ^{186}Au to spins of $24\hbar$ and $23\hbar$, respectively. As shown clearly in earlier studies of Au ground-state properties, there is a marked oblate-prolate change in shape between the two isotopes.

Two new strongly coupled prolate bands have been observed in ^{186}Au. Their appearance in ^{186}Au but not in ^{188}Au is understandable in view of the ground-state shape transition known to occur at $N = 107$. The yrast band of ^{186}Au, which shows no gain in alignment through $\hbar\omega \simeq 0.40$ MeV, is interpreted as a $\pi h_{9/2} \otimes \nu i_{13/2}$ configuration. Both primary band crossings thought to occur in this region, those due to the $\nu i_{13/2}$ AB and $\pi h_{9/2}$ ef alignments, are thus blocked. By comparison, the second strongly coupled structure, assigned a $\pi i_{13/2} \otimes \nu i_{13/2}$ configuration, exhibits a crossing at $\hbar\omega \simeq 0.23$ MeV, attributed to the alignment of a pair of $h_{9/2}$ quasiprotons.

Oblate $\nu i^{-1}_{13/2} \otimes \pi h^{-1}_{11/2}$ structures, analogous to those well known in the $^{190-194}$Au nuclei, have been established. The ^{186,188}Au energy staggering and signature inversion characteristics of those bands follow the systematic behavior observed in the heavier isotopes. The signature inversion effect can be qualitatively explained in terms of deviations from the $\gamma = -60°$ oblate symmetry axis, which in turn affect the signature splitting of the $\nu i_{13/2}$ orbital. However, the magnitude of the inversion and its variation over a range of neutron numbers is still not understood.

In the 11^- band of ^{188}Au, a sharp alignment gain at $\hbar\omega = 0.31$ MeV is most likely due to the $\nu i_{13/2}$ BC crossing. As well, all of the $^{186-194}$Au $\nu i^{-1}_{13/2} \otimes \pi h^{-1}_{11/2}$ bands reveal hints of a gain in alignment at $\hbar\omega \simeq 0.35$ MeV, which could represent the onset of $\nu i_{13/2}$ CD, AD alignments. It appears that a complete picture of the oblate band crossings cannot be obtained without a more extensive knowledge of these structures.

Four-quasiparticle oblate band structures built on 15^+ states have been populated in both nuclei. Their characteristics fit very well-known systematic features in the heavier odd-odd Au isotopes, previously interpreted as $\nu i^2_{13/2} \otimes \pi h_{11/2} \otimes$ "νj" configurations ($\nu j = \nu p_{3/2}$ or $\nu f_{5/2}$).

Measured average values of the $B(M1; I \rightarrow I-1)/B(E2; I \rightarrow I-2)$ ratios for bands in ^{186,188}Au have been interpreted by extending the geometrical formalism of Dönau and Frauendorf to odd-odd nuclei. However, within that model the experimental absence of odd-even-I staggering in the ratios for the ^{186}Au oblate band is not compatible with the observed energy staggering, since in the theory the two features are inextricably linked. $B(M1)/B(E2)$ ratios for the ^{186}Au prolate bands have also been interpreted within the extended geometrical framework. In the $\pi i_{13/2} \otimes \nu i_{13/2}$ case the experimental values vary little as a function of spin, a surprising feature which, however, is shown to be consistent with a suggested $\pi h_{9/2}$ crossing.

ACKNOWLEDGMENTS

This work has been supported by the U.S. Department of Energy, under Contract No. DE-SG05-87ER40361, by the Canadian Natural Sciences and Engineering Research Council, and by AECL Research.

[1] A.J. Larabee, M.P. Carpenter, L.L. Riedinger, L.H. Courtney, J.C. Waddington, V.P. Janzen, W. Nazarewicz, J.-Y. Zhang, R. Bengtsson, and G.A. Leander, Phys. Lett. **169B**, 21 (1986).

[2] R. Bengtsson, T. Bengtsson, J. Dudek, G. Leander, W. Nazerewicz, and J.-Y. Zhang, Phys. Lett. B **183**, 1 (1987).

[3] K. Wallmeroth, G. Bollen, A. Dohn, P. Egelhof, J. Grüner, F. Lindenlauf, U. Krönert, J. Campos, A. Rodriguez Yunta, M.J.G. Borge, A. Venugopalan, J.L. Wood, R.B. Moore, and H.J. Kluge, Phys. Rev. Lett. **58**, 1516 (1987).

[4] V.P. Janzen, M.P. Carpenter, L.L. Riedinger, W. Schmitz, S. Pilotte, S. Monaro, D.D. Rajnauth, J.K. Johansson, D.G. Popescu, J.C. Waddington, Y.S. Chen, F. Dönau, and P.B. Semmes, Phys. Rev. Lett. **61**, 2073 (1988).

[5] A.J. Kreiner, J. Davidson, M. Davidson, P. Thieberger, and E.K. Warburton, Phys. Rev. C **42**, 878 (1990).

[6] J.K. Johansson, D.G. Popescu, D.D. Rajnauth, J.C. Waddington, M.P. Carpenter, L.H. Courtney, V.P. Janzen, A.J. Larabee, Z.M. Liu, and L.L. Riedinger, Phys. Rev. C **40**, 132 (1989).

[7] M.P. Carpenter, C.R. Bingham, L.H. Courtney, V.P. Janzen, A.J. Larabee, Z.-M. Liu, L.L. Riedinger, W. Schmitz, R. Bengtsson, T. Bengtsson, W. Nazarewicz, J.-Y. Zhang, J.K. Johansson, D.G. Popescu, J.C. Waddington, C. Baktash, M.L. Halbert, N.R. Johnson, I.Y. Lee, Y. S. Schutz, J. Nyberg, A. Johnson, J. DeBuc, S. Monaro, S. Pilotte, K. Honkanen, D.G. Sarantites, and

D.R. Haenni, Nucl. Phys. **A513**, 125 (1990).
[8] J. Nyberg, A. Johnson, M.P. Carpenter, C.R. Bingham, L.H. Courtney, V.P. Janzen, S. Juutinen, A.J. Larabee, Z.-M. Liu, L.L. Riedinger, C. Baktash, M.L. Halbert, N.R. Johnson, I.Y. Lee, Y. Schutz, J.C. Waddington, and D.G. Popescu, Nucl. Phys. **A511**, 92 (1990).
[9] S. Pilotte, G. Kajrys, S. Monaro, M.P. Carpenter, V.P. Janzen, L.L. Riedinger, J.K. Johansson, D.G. Popescu, D.D. Rajnauth, and J.C. Waddington, Phys. Rev. C **40**, 610 (1989).
[10] F. Hannachi, G. Bastin, M.G. Porquet, C. Schück, J.P. Thibaud, C. Bourgeois, L. Hildingsson, D. Jerrestam, N. Perrin, H. Sergolle, F.A. Beck, T. Byrski, and J.C. Merdinger, Nucl. Phys. **A481**, 135 (1988).
[11] A.J. Kreiner, J. Davidson, M. Davidson, P. Thieberger, E.K. Warburton, S. André, and J. Genevey, Nucl. Phys. **A489**, 525 (1988).
[12] A.J. Kreiner, Nucl. Phys. **A520**, 225c (1990).
[13] A.J. Kreiner, V.R. Vanin, F.A. Beck, Ch. Bourgeois, Th. Byrski, D. Curien, G. Duchêne, B. Haas, J.C. Merdinger, M.G. Porquet, P. Romain, S. Rouabah, D. Santos, and J.P. Vivien, Phys. Rev. C **40**, R487 (1989).
[14] F. Dönau and S. Frauendorf, in *Proceedings of the Conference on High Angular Momentum Properties of Nuclei*, Oak Ridge, TN, 1982, edited by N.R. Johnson (Harwood, New York, 1983), p.143.
[15] F. Dönau, Nucl. Phys. **A471**, 469 (1987).
[16] A.J. Kreiner, J. Davidson, M. Davidson, D. Abriola, C. Pomar, and P. Thieberger, Phys. Rev. C **36**, 2309 (1986); *ibid.* **37**, 1338(E) (1988).
[17] A. Neskakis, R.M. Lieder, H. Beuscher, Y. Gono, D.R. Haenni, and M. Müller-Veggian, Nucl. Phys. **A390**, 53 (1982).
[18] A. Neskakis, R.M. Lieder, H. Beuscher, Y. Gono, D.R. Haenni, M. Müller-Veggian, and C. Mayer-Böricke, Phys. Lett. **80B**, 194 (1979).
[19] G. Palameta and J.C. Waddington, Nucl. Instrum. Methods **A234**, 476 (1985).
[20] M.A. Deleplanque, C. Gerschel, M. Ishihara, C. Bourgeois, M.G. Desthuilliers, N. Perrin, J.P. Husson, P. Kilcher, J. Letessier, and V. Berg, J. Phys. (Paris) **36**, L-205 (1975).
[21] S. Pilotte, Ph.D. thesis, Université de Montréal, 1987.
[22] V. Berg, Z. Hu, J. Oms, and C. Ekström, Nucl. Phys. **A410**, 445 (1983).
[23] C. Bourgeois, P. Kilcher, J. Lettessier, V. Berg, and M.G. Desthuilliers, Nucl. Phys. **A295**, 424 (1978).
[24] M.A. Deleplanque, C. Gerschel, N. Perrin, and V. Berg, Nucl. Phys. **249**, 366 (1975).
[25] C. Ekström, I. Lindgren, S. Ingelman, M. Olsmats, and G. Wannberg, Phys. Lett. **60B**, 146 (1976).
[26] C. Ekström, L. Robertsson, S. Ingelman, and I. Ragnarsson, Nucl. Phys. **A348**, 25 (1980).
[27] M.C. Abreu, V. Berg, K. Fransson, A. Höglund, J. Oms, and M.G. Porquet, Nucl. Phys. **A437**, 324 (1985).
[28] A. Neskakis, H. Beuscher, B. Bochev, R.M. Lieder, T. Morek, and F.R. May, *Proceedings of the International Conference on Nuclear Physics*, Florence, Italy, 1983 (Tipografia Compositori, Bologna, 1983) Vol. 1, p. 71.
[29] M.G. Porquet, C. Bourgeois, P. Kilcher, and J. Sauvage-Letessier, Nucl. Phys. **A411**, 65 (1983).
[30] M.G. Porquet, Ph.D. thesis, Université de Paris-Sud, Centre d'Orsay, 1981.
[31] G. Liljegren, I. Lindgren, L. Sanner, and K.E. Adelroth, Ark. Fys. **25**, 107 (1964).
[32] Y.W. Chan, V.J. Ehlers, and W.A. Nierenberg, Phys. Rev. **144**, C1020 (1966).
[33] G.H. Fuller, J. Phys. Chem. Ref. Data **5**, 835 (1976).
[34] H. Rubinsztein and M. Gustafsson, Phys. Lett. **58B**, 283 (1975).
[35] D. Vandeplassche, E. van Walle, J. Wouters, N. Severijns, and L. Vanneste, Hyp. Int. **22**, 483 (1985).
[36] Y. Gono, R.M. Lieder, M. Müller-Veggian, A. Neskakis, and C. Mayer-Böricke, Phys. Lett. **70B**, 159 (1977).
[37] M.O. Kortelahti, E.F. Zganjar, H.K. Carter, C.D. Papanicolopulos, M.A. Grimm, and J.L. Wood, J. Phys. G **14**, 1361 (1988).
[38] B. Roussiere, C. Bourgeois, P. Kilcher, J. Sauvage, and M.G. Porquet, Nucl. Phys. **A438**, 93 (1985).
[39] B. Roussiere, C. Bourgeois, P. Kilcher, J. Sauvage, M.G. Porquet, A. Wojtasiewicz, and the ISOCELE Collaboration, Nucl. Phys. **A485**, 111 (1988).
[40] Y.A. Ellis-Akovali, Nucl. Data Sheets **36**, 559 (1982).
[41] E.F. Zganjar and J.L. Wood, Hyperfine Interact. **43**, 321 (1988); and J.L. Wood, private communication (1990).
[42] M. Piiparinen, S.K. Sah, P.J. Daly, C.L. Dors, F.M. Bernthal, and T.L. Khoo, Phys. Rev. C **13**, 2208 (1976).
[43] A. BenBraham, V. Berg, C. Bourgeois, P. Kilcher, J. Letessier, M.G. Desthuillers-Porquet, C. Schück, A. Huck, A. Knipper, C. Richard-Serre, and A. Höglund, Nucl. Phys. **A332**, 397 (1979).
[44] G. Kajrys *et al.* (unpublished).
[45] R.B. Firestone, Nucl. Data Sheets **34**, 537 (1981).
[46] J.L. Wood, private communication (1990).
[47] R. Bengtsson and S. Frauendorf, Nucl. Phys. **A314**, 27 (1979); **A327**, 139 (1979).
[48] D. Santos, A.J. Kreiner, J. Davidson, M. Davidson, M. Debray, D. Hojman, and G. Falcone, Phys. Rev. C **39**, 902 (1989).
[49] F. Hannachi, G. Bastin, M.G. Porquet, J.P. Thibaud, C. Bourgeois, L. Hildingsson, N. Perrin, H. Sergolle, F.A. Beck, and J.C. Merdinger, Z. Phys. A **330**, 15 (1988).
[50] A. Neskakis, R.M. Lieder, M. Müller-Veggian, H. Beuscher, W.F. Davidson, and C. Mayer-Böricke, Nucl. Phys. **A261**, 189 (1976).
[51] R.M. Lieder, G. Sletten, J. Borgreen, and J. Pedersen, Nucl. Phys. **A375**, 291 (1982).
[52] S. Frauendorf, L.L. Riedinger, J.D. Garrett, J.J. Gaardhøje, G.B. Hagemann, and B. Herskind, Nucl. Phys. **A431**, 511 (1984).
[53] J.D. Garrett, J. Nyberg, C.H. Yu, J.M. Espino, and M.J. Godfrey, in *Proceedings of the International Conference on Contemporary Topics in Nuclear Structure Physics*, edited by R. Casten, A. Frank, M. Moshinsky, and S. Pittel (World Scientific, Singapore, 1988), p. 699.
[54] R. Bengtsson, H. Frisk, F.R. May, and J.A. Pinston, Nucl. Phys. **A415**, 189 (1984).
[55] F. Dönau and F.-R. May, in *Proceedings of the International Conference on Nuclear Shapes*, Pelagia, Greece, 1987, edited by J. D. Garrett (World Scientific, Singapore, Singapore, 1988), p. 444.
[56] A. Ikeda and T. Shimano, Phys. Rev. Lett. **63**, 139 (1989).
[57] G.A. Leander, S. Frauendorf, and F.-R. May, in *Proceedings of the Conference on High Angular Momentum Properties of Nuclei*, Oak Ridge, TN, 1982, edited by N.R. Johnson (Harwood, New York, 1983), p. 281.
[58] H. Hübel, A.P. Byrne, S. Ogaza, A.E. Stuchbery, G.D.

Dracoulis, and M. Guttormsen, Nucl. Phys. **A453**, 316 (1986).
[59] M. Guttormsen, K.P. Blume, Y.K. Agarwal, A. v Grumbkow, K. Hardt, H. Hübel, J. Recht, and P. Schüler, Z. Phys. **A312**, 155 (1983).
[60] A.J. Larabee, L.H. Courtney, S. Frauendorf, L.L. Riedinger, J.C. Waddington, M.P. Fewell, N.R. Johnson, I.Y. Lee, and F.K. McGowan, Phys. Rev. C **29**, 1934 (1984).
[61] R. Ma, E.S. Paul, C.W. Beausang, S. Shi, N. Xu, and D.B. Fossan, Phys. Rev. C **36**, 2322 (1987).
[62] M.J. Godfrey, Y. He, I. Jenkins, A. Kirwan, P.J. Nolan, D.J. Thornley, S.M. Mullins, and R. Wadsworth, J. Phys. G **15**, 487 (1989).
[63] C.W. Beausang, L. Hildingsson, E.S. Paul, W.F. Piel, Jr., N. Xu, and D.B. Fossan, Phys. Rev. C **36**, 1810 (1987).
[64] E.S. Paul, C.W. Beausang, D.B. Fossan, R. Ma, W.F. Piel, Jr., and N. Xu, Phys. Rev. C **36**, 1853 (1987).
[65] J. Kern and G.L. Struble, Nucl. Phys. **A286**, 371 (1977).
[66] U. Garg, A. Chaudhury, M. Drigert, E. Funk, J. Mihelich, D. Radford, H. Helppi, R. Holzmann, R. Janssens, T.L. Khoo, A.M. Van den Berg, and J.L. Wood, Phys. Lett. B **180**, 319 (1986).
[67] H. Toki, H.L. Yadav, and A. Faessler, Z. Phys. A **292**, 79 (1979); H.L. Yadav, H. Toki, and A. Faessler, Phys. Lett. **81B**, 119 (1979).